AFRL-OSR-VA-TR-2014-0201

UNCONVENTIONAL HIGH DENSITY VERTICALLY ALIGNED CONDUCTING POLYMER

QIMING ZHANG
PENNSYLVANIA STATE UNIVERSITY

08/25/2014
Final Report

Air Force Research Laboratory
AF Office Of Scientific Research (AFOSR)/RTD
Arlington, Virginia 22203
Air Force Materiel Command

REPORT DOCUMENTATION PAGE

Form Approved
OMB No. 0704-0188

PLEASE DO NOT RETURN YOUR FORM TO THE ABOVE ORGANIZATION.

1. REPORT DATE *(DD-MM-YYYY)*	2. REPORT TYPE	3. DATES COVERED *(From - To)*
22-08-2014	Final Report	Aug. 15, 2011 - Aug. 14, 2014

4. TITLE AND SUBTITLE
Unconventional High Density Vertically Aligned Conducting Polymer

5a. CONTRACT NUMBER

5b. GRANT NUMBER
FA9550-11-1-0192

5c. PROGRAM ELEMENT NUMBER

6. AUTHOR(S)
Zhang, Qiming, The Pennsylvania State University
Wardle, Brian, L. - Massachusetts Institute of Technology

5d. PROJECT NUMBER

5e. TASK NUMBER

5f. WORK UNIT NUMBER

7. PERFORMING ORGANIZATION NAME(S) AND ADDRESS(ES)
The Pennsylvania State University
Office of Sponsored Programs
110 Technology Center Building
University Park, PA 16802-7000

8. PERFORMING ORGANIZATION REPORT NUMBER

9. SPONSORING/MONITORING AGENCY NAME(S) AND ADDRESS(ES)
Dr. Charles Lee
AFOSR/RSA
875 North Randolph Street
Suite 325, Room 3112
Arlington, VA 22203

10. SPONSOR/MONITOR'S ACRONYM(S)

11. SPONSOR/MONITOR'S REPORT NUMBER(S)

12. DISTRIBUTION/AVAILABILITY STATEMENT
Unlimited

13. SUPPLEMENTARY NOTES

14. ABSTRACT

Supercapacitors are promising energy storage devices due to their higher energy density than dielectric capacitors and higher power density and long cycle life time (> millions) compared with conventional batteries. In order to meet the demands of a wide range of energy technologies, supercapacitors with higher energy and power densities are required. Although many past research programs have focused mainly on gravimetric energy densities, in this program, we have also devoted efforts to study and develop nano-morphologic structures to realize high volumetric energy and power densities, since device volume is another critical and key performance parameter. Fundamental studies have been carried out on the mobile ion transport and storage in the nano-structures developed in this program. In order to meet different application requirements and also for fundamental studies of ion transport and storage in nano-porous media, this program selected carbon based electrodes with unique and controlled nano-morphologies: highly aligned carbon nanotubes (A-CNT) and graphene. This program also developed the conformal nm-scale coating of conducting polymer on A-CNTs, which as the pseudocapacitor electrodes store charges through the whole volume, thus leading to potential of even

15. SUBJECT TERMS

16. SECURITY CLASSIFICATION OF:			17. LIMITATION OF ABSTRACT	18. NUMBER OF PAGES	19a. NAME OF RESPONSIBLE PERSON
a. REPORT	b. ABSTRACT	c. THIS PAGE			19b. TELEPHONE NUMBER *(Include area code)*

Reset

Final Technical Report

UNCONVENTIONAL HIGH DENSITY VERTICALLY ALIGNED CONDUCTING POLYMER

Period Covered: August 15, 2011 to August 15, 2014

AFOSR Program No. FA9550-11-1-0192

Program Manager: Dr. Charles Lee

e-mail: charles.lee@afosr.af.mil, Ph: (703) 696-7779

Submitted by

Qiming Zhang

The Pennsylvania State University, University Park, PA 16802

Brian L. Wardle

Massachusetts Institute of Technology, Cambridge, MA 02139

August 21, 2014

Summary:

Electric energy storage devices are of prime importance for a broad range of DoD and AirForce applications. Supercapacitors are promising energy storage devices due to their higher energy density than dielectric capacitors and higher power density and long cycle life time (> millions) compared with conventional batteries. In order to meet the demands of a wide range of energy technologies, supercapacitors with higher energy and power densities are required. Although many past research programs have focused mainly on gravimetric energy densities, in this program, we have also devoted efforts to study and develop nano-morphologic structures to realize high volumetric energy and power densities, since device volume is another critical and key performance parameter. Fundamental studies have been carried out on the mobile ion transport and storage in the nano-structures developed in this program.

In order to meet different application requirements and also for fundamental studies of ion transport and storage in nano-porous media, this program selected carbon based electrodes with unique and controlled nano-morphologies: highly aligned carbon nanotubes forests (A-CNTs) and graphene. As synthesized A-CNTs have low volume fraction of CNT (~ 1 %). Traditional method to achieve high volumetric performance of A-CNTs was to employ liquid surface tension densification, which did not have control on the nanomorphology of A-CNTs after densification. In this program, making use of and improving upon the mechanical densification method developed at Co-PI's group at MIT, we achieved 40% volumetric density of A-CNTs. A series of supercapacitor electrodes have been developed and characterized. As can be seen in the report, the high volume fraction of A-CNTs and highly aligned ion channels in the nano-porous electrodes lead to the superior performance of the supercapacitors compared with any CNT based supercapacitors electrodes studied earlier. The supercapacitors exhibit a volumetric power density, 25 kW/L (and gravimetric power density 50 kW/kg) for the capacitor cell with 0.8 mm thick A-CNTs, compared with the similar capacitors using A-CNTs densified by the liquid collapsing method, 13.4 kW/L (24 kW/kg) for cells with 0.5 mm thick A-CNTs. The study also shows the importance of the ionic conductivity of electrolytes in controlling the power and energy densities of the supercapacitors.

We have devoted efforts to develop and investigate electric double layer capacitors (EDLCs) based on ultra-high density a-graphene. It is noted that although very large gravimetric capacitances, as high as 200 F/g, has been reported for the graphene EDLCs, the volumetric properties as a more useful and practical metric has been overlooked. The very high density (1.15 g/cm^3) aligned nanoporous graphene networks (A-NPG) by a self-assembly method developed here were investigated for the electrodes for EDLCs, which demonstrated very large volumetric capacitance of 197 F/cm^3 for A-NPG. Additionally, the supercapacitors exhibited very high volumetric energy and power densities, 75 Wh/L and 510 kW/L. Although the energy density is a little lower than that of the asymmetric supercapacitors, the EDLC based A-aMEGO supercapacitors show very high power density, which demonstrate the superior performance of graphene based supercapacitors and enable this new class of electrodes to be considered for practical energy storage applications.

In this program, we have also developed another nano-morphology for nano-porous electrodes: nm-scale conformal coating of a conducting polymer, poly(ethylenedioxythiophene) (PEDOT) on aligned carbon nanotubes (A-CNTs). In contract to the electric double layer capacitors (EDLC) which store charges on the surface of the electrodes, conducting polymer (CP) layers store charge in the entire volume, which hence provide opportunity to significantly enhance the volumetric performance of the energy storage devices. A-CNTs provide mechanical support of CP layers for long cycle life and aligned ion channels for efficient ion transport. Cyclic voltammetry and galvanostatic studies, as well as electric impedance spectroscopy study, all point out the significantly improved capacitive performance of the CP-coated A-CNTs electrodes compared with the pure carbon based electrodes. Moreover, compared with supercapacitors with CP coated on random CNTs which shows 90% capacitor retention after 1000 cycles,

the conformally coated CP on A-CNTs electrodes show robust mechanical stability and maintain near 100% retention after 1000 charge/discharge cycles.

Operation temperature is another important parameter for energy storage devices. For supercapacitors, the electrolyte is the most critical component that controls the temperature behavior of the capacitors. Here we introduce a new eutectic mixtures of electrolytes (ionic liquids), for example, BMI BF_4 and BMP BF_4, and show that the operation temperature, especially the low temperature operation capability of the supercapacitors can be significantly improved. Compared with the melting of 1-Butyl-3-methylimidazolium tetrafluoroborate (BMI BF_4) and 1-butyl-4-methylpyridinium tetrafluoroborate (BMP BF_4), which is at -30 ^oC and -39 ^oC, respectively, in the eutectic mixture, the melting is lowered to -74 ^oC.

In this report, the capacitor performances for these nanoporous electrodes are summarized. It should be noted that since the power density is directly affected by the ion transport time through the electrodes, the thick electrodes may show lower "apparent" power density compared with the thinner electrodes. For example, the electrode thickness for each electrode in the high volume density (40 vol%) A-CNTs is 0.8 mm, while for the A-aMEGO (nano-porous graphene) electrode, the electrode thickness is in 0.1 mm (100 μm). In the conformally CP-coated-A-CNTs, the electrode thickness is 0.2 mm. On the other hand, in the Ragone plots, the comparisons among different supercapacitors are made for the electrodes with similar thickness.

Since the energy and power densities of supercapacitors are directly proportional to the square of cell operation voltage V (~ V^2), raising the cell operation voltage will have great potential to enhance the energy and power densities. Asymmetric supercapacitors, which allow for optimization of both cathode and anode simultaneously, provide an attractive approach to raise the cell operation voltage, besides other properties. In this program, we have investigated asymmetric supercapaictor configurations for carbon based electrodes for cathode and CP-coated A-CNTs for anode, based on their electrochemical windows.

Here, we exploit the asymmetric supercapacitors, allowing both electrodes to be separately tailored, increasing device capacitance and the electrochemical window, and thereby operating voltage. The conformal vapor deposited conducting polymer coating enhances the charge storage of the anode, while the underlying aligned nanowire morphology provides direct non-tortuous fast ion transport pathways to enhance power. The a-graphene cathode, fabricated via a self-assembly process, shows the highest active material density of 1.15 g/cm^3, which, when combined with a high specific surface area of 3,000 m^2/g, yields highest specific volumetric capacitance, energy and power densities for the cathode, among all the carbon based electrodes. As a result, the asymmetric supercapacitors show an energy density 113 Wh/L (176 Wh/kg), which are the highest among all carbon based spercapacitors, and a power density 149 kW/L (233 kW/kg). (the electrode thickness for the anode is 0.2 mm (CP coated A-CNTs) and for the cathode is 0.1 mm)

During the third year of this program, an asymmetric supercapacitor exploiting well-characterized nm-scale conformal coating of PEDOT on A-CNTs as the negative electrode and the ultrahigh density A-CNTs as the positive electrode was developed. Both electrodes were tailored separately to extend the cell operation potential to 4 V in 2 M $BMIBF_4$/propylene carbonate (PC) electrolyte, leading to 130.6 kW L^{-1} and 82.8 Wh L^{-1} in volumetric performance and 269.4 kW kg^{-1} and 170.7 Wh kg^{-1} in gravimetric performance, respectively. In addition, a new and accurate method (QV curve) was introduced to measure the energy storage efficiency of the asymmetric cell. An equivalent circuit model was developed based on the EIS, revealing the difference in working mechanisms between EDLC and pseudocapacitor and demonstrating the optimized asymmetric design, which leads to the high cell performance. (The electrode thickness for the anode is 0.21 mm and for the cathode is 0.25 mm).

1. Symmetric supercapacitors with controlled unique nanomorphology

1.1 Development and characterization of supercapacitors with ultra-high volume fraction (40%) A-CNTs: Effect of A-CNT volume fraction and electrolytes on the performance

Presently, most supercapacitors are fabricated from activated carbon (AC) which possesses a very large specific surface area (1000 to 2000 m^2/g). Recent advances have demonstrated many attractive features of utilizing aligned carbon nanotubes (A-CNTs) for supercapacitors nanoporous electrodes, especially the parallel ion channels formed by the A-CNTs that improve the ion transport, as schematically illustrated in Figure 1(a), compared with randomly arranged nanoporous electrodes from AC, forming tortuous ion transport pathways. Consequently, supercapacitor cells with A-CNTs exhibit higher power and energy density than that from AC. Since as grown A-CNT forests have CNT volumetric density < 5 vol%, A-CNTs should be densified to reach higher A-CNT volumetric density for practical supercapacitor applications. In the past decade, many works have been conducted to produce aligned A-CNTs with high CNT density to achieve high volumetric capacitance, energy density, and power density, which are critical for modern electric and electronic systems to realize compact device size and increased functions within given device volumes. For example, Futaba et al. introduced a liquid collapsing method to densify A-CNTs in which the surface tension of liquid forces the A-CNTs to collapse to a high density (~50 vol%). Compared with the liquid densification method, the mechanical densification method developed at our laboratory at MIT offers several advantageous. This method provides a precise control on the density of the final A-CNTs, ranging from the original 1 vol% A-CNTs to more than 50 vol%. Besides, A-CNT samples with different sizes can be densified with precisely controlled nanomorphology (alignment) and hence this method provides a realistic pathway for scaling up high density A-CNTs for large scale manufacturing of supercapacitors from A-CNTs of ultra-high volume density. In addition, the availability of A-CNTs with different density and hence different ion channel sizes also creates a great opportunity to study how the ion channel size formed by the A-CNTs affect ion transport and storage which is of great importance in developing supercapacitors with high energy, power density, and tailored performance.

We have been developing and characterizing supercapacitors fabricated from A-CNTs in the volume fraction from 1% to 40%. These ACNTs are densified employing the mechanical densification scheme developed in MIT. We study how the energy and power density, equivalent series resistance (ESR) of the cell, and specific capacitance evolve as the A-CNT volume fraction is increased from 1 vol% to 40 vol%. The results demonstrate the advantage of the A-CNTs using mechanical densification method in providing much better nonamorphology for ion transport compared with that using the liquid collapsing method. As a result, the supercapacitors here exhibit a much higher volumetric power density, 25 kW/L (50 kW/kg) for the capacitor cell with 0.8 mm thick A-CNTs, compared with the similar capacitors using A-CNTs densified by the liquid collapsing method, 13.4 kW/L (24 kW/kg) for cells with 0.5 mm thick A-CNTs.

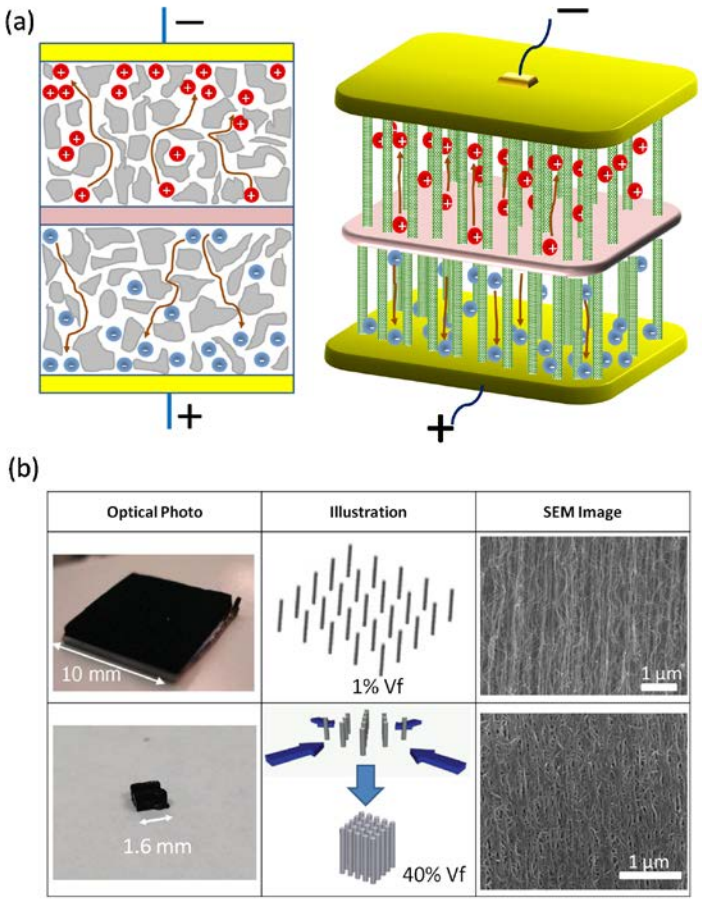

Figure1.a) Schematic of the tortuous ion transport paths in nanoporous electrodes formed, for example, from the activated carbons, and parallel ion pathways in the A-CNTs. b) Optic images, schematic of mechanical densification process, and SEM images of 1% Vf and 40% Vf A-CNTs.

During the first year, we have also been studying the influence of the ionic conductivity of electrolyte on the electrochemical performance of the supercapacitors. An imidazolium based ionic liquid, (1-ethyl-3-methylimidazolium-tetrafluoroborate**,** EMI-BF_4), was chosen for the study. Imidazolium ionic liquids (ILs) due to their high ionic conductivity and wide electrochemical window have been investigated very extensively as the electrolytes for supercapacitors. Recent studies have also shown that a mixture of an IL such as EMI-BF_4 and molecular liquid such as propylene carbonate (PC) can lead to marked enhancement (more than two times higher) in the ionic conductivity compared with the pure EMI-BF_4. The experimental results show that increased ionic conductivity of the electrolyte can lead to a large increase in the power density (more than double the power density using EMI-BF_4/PC compared with pure EMI-BF_4) of the supercapacitors.

The A-CNTs in this study were synthesized via a modified chemical vapor deposition (CVD) method on silicon substrates using iron (Fe) on alumina as a catalyst. The as-grown A-CNT forests have a 1% volume fraction (Vf) of CNTs with densities of 10^9–10^{10} CNTs cm^{-2}. The average diameter of these CNTs is 8 nm with 3-5 shells of walls and the CNT-CNT spacing is approximately 80 nm in the as-grown A-

CNT forests. For the high volume fraction A-CNT fabrication, the CNT forests were released from the silicon substrate and then subjected to a mechanical biaxial densification process in two orthogonal directions as illustrated in Figure 1b. In this method, the released A-CNT forests were placed in a specially designed sample holder. The height of the sample holder was the same as the height of the A-CNT forest so that the top and bottom of the forest remained flat during the densification process. The A-CNT forest was densified along one direction first (see Figure 1b) to a fixed amount using a mechanical bar, and then another mechanical bar in the orthogonal direction was used to press the A-CNT forest to the final density. (The densifications in the two directions were the same for the A-CNTs studied in this paper). By varying the inter-CNT distance in densification process, A-CNT forests with different volume fractions can be achieved. The density of the 40% Vf A-CNTs is 0.52 gcm^{-3}, determined by directly measuring the weight and volume of the electrode.

The A-CNT forests (0.8 mm thickness) were used as the electrodes of the supercapacitors. Thick A-CNT samples are easier to characterize and handle. An ionic liquids/molecular liquids (IL/ML) mixture, 3 M EMI-BF_4 (1-ethyl-3-methylimidazolium tetrafluoroborate)/PC (propylene carbonate), was used as the electrolyte which has a higher ionic conductivity compared with that of pure ionic liquid EMI-BF_4. A 25 mm thick polypropylene porous membrane (Celgard 3501, Celgrad LLC) was used as the separator which is chemical stable in IL/ML mixture. The A-CNT/separator/A-CNT unit was placed between two pieces of Au coated steel plates (2 mm x 2 mm x 1.6 mm) which served as the current collectors, and the whole assembly was housed in a Teflon cell. As a comparison, supercapacitor electrodes of the activated carbon powders (Sigma-Aldrich) with 10 wt% PTFE and 10 wt% carbon black were also fabricated using the standard method repeated in the literature. Since the charge/discharge times of supercapacitors depend on the electrode thickness, in addition to the electrode nanomorphology, the activated carbon electrodes and the A-CNT electrodes had the same dimensions for the supercapacitor performance comparison.

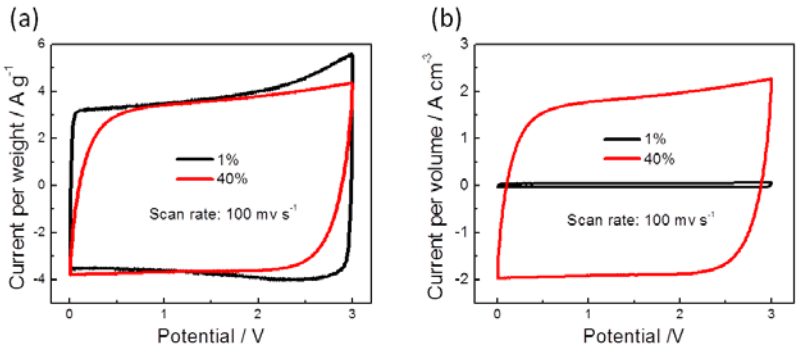

Figure 2. Electrochemical performance of supercapacitors with A-CNT electrodes and EMI-BF_4/PC electrolyte at 4 V: a) gravimetric cyclic voltammograms and b) volumetric cyclic voltammograms of A-CNT electrodes with 1% and 40% Vf at 100 mVs^{-1}.

Figure 2a presents the cyclic voltammetry (CV) curves at 100 mVs^{-1} scan rate of supercapacitors with 1% Vf and 40% Vf of A-CNTs as electrodes in3 MEMI-BF_4/PC electrolyte. The specific capacitance of supercapacitors can be calculated by integrating the CV curve in half cycle. As shown in figure 2a, there is very little drop of the gravimetric capacitance as the A-CNT volume fraction increases from 1% Vf to 40% Vf, indicating that the densification process maintains the nanomorphology of parallel ion pathways formed by the A-CNTs. On the other hand, increasing the A-CNTs volume fraction from 1% to 40%

results in a marked increase in the volumetric capacitance, as shown in Figure 2b. Since there is no faradic reaction in these supercapacitors, the curves exhibit symmetric charge and discharge rectangular shape, showing ideal capacitive behavior.

The galvanostatic cycles between 0 and 4 V for the supercapacitors with 1% Vf and 40% VfA-CNT electrodes under 1 Ag^{-1} current density are presented in Figure 3a.From the slope of the galvanostatic curves, *dV*/*dt*, the capacitance of the cell can be determined:

$$C = I / (dV / dt) \tag{1}$$

where *I* is the constant current density, *V* is potential, and *t* is discharge time. Figure3b and Figure 3c present the specific gravimetric and volumetric capacitances at different discharge currents, respectively. Although the electrodes with 1% Vf of A-CNTs show a very high specific gravimetric capacitance, >270 Fg^{-1}, their volumetric capacitance is very low (~ 3 F cm^{-3}).

It should be pointed out that the 1% Vf A-CNTs have a very low active material density of 0.013 g/cm^3. For electrodes with such a low active material density, the majority of the electrode volume is filled with electrolytes whose weight is not included in evaluating the gravimetric electrochemical performance. Hence, as pointed out by Gogotsi and Simon, the gravimetric data for electrodes with very low active material density do not provide meaningful information of the practical electrochemical performance of package supercapacitors. Instead, the volumetric values should be used when comparing electrodes with large difference in the active material density. For the purpose of illustration, the gravimetric electrochemical performance data are still presented for the electrodes with 1% Vf A-CNTs besides the volumetric values. The specific volumetric capacitance of 40% Vf A-CNT electrodes is about 40 times higher than that of 1% Vf A-CNT electrodes, indicating that the mechanical densification method developed here preserves the nanomorphology of the A-CNTs.

From the capacitance and the equivalent series resistance (ESR), the power density and energy density of the supercapacitors can be obtained. The Ragone plots for the supercapacitor cells under 4 V were presented in Figure 3d and Figure 3e. The energy of the cell in each discharging cycle, *E*, is determined by integrating the discharge curves,

$$E = \int IV(t)dt \tag{2}$$

The equivalent series resistance (ESR) is determined from

$$ESR = \Delta V / \Delta I \tag{3}$$

where ΔV is the voltage drop as the current is switched from a positive value to a negative value, such as from 1 Ag^{-1} to -1 Ag^{-1} (ΔI=2 Ag^{-1}). The power density, hence, can be deduced from

$$P = V^2 / (4 * ESR) \tag{4}$$

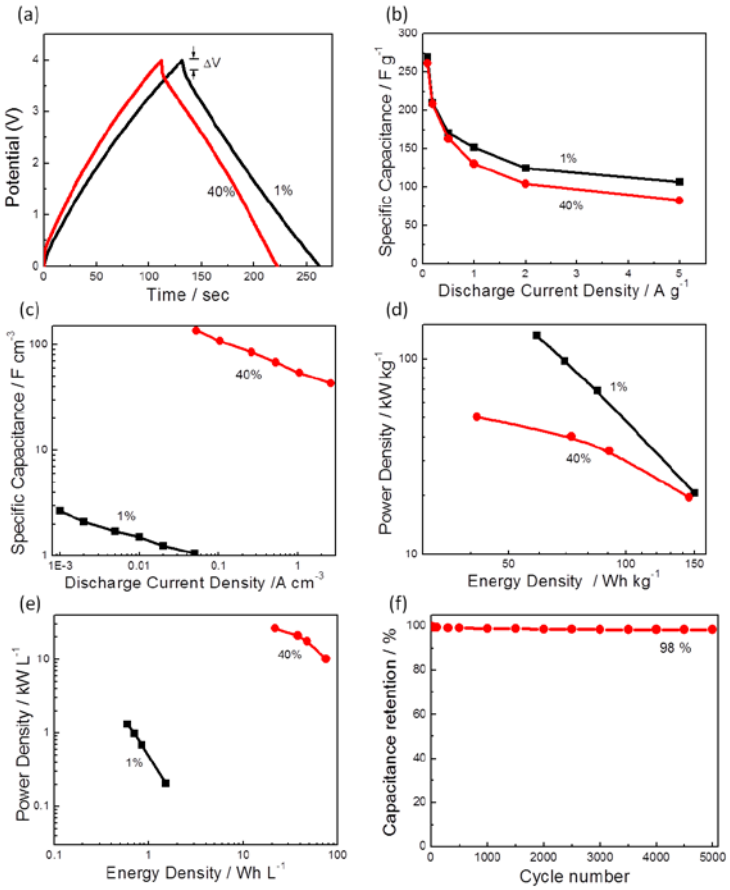

Figure 3. a) Galvanostatic charge discharge curves at 1 Ag^{-1} for supercapacitors with electrodes of 1% and 40% Vf A-CNTs and EMI-BF_4/PC electrolyte. b) Gravimetric and c) volumetric specific capacitance for the supercapacitors with electrodes of 1%and 40% Vf A-CNTs at different discharge rates. d) Gravimetric and e) volumetric Ragone plots for the supercapacitors with electrodes of 1%and 40% Vf A-CNTs. f) Cycle performance of 40% Vf A-CNTs supercapacitor with a voltage of 4 V at charge and discharge current density of 5 A g^{-1}.

The active material density of the electrodes in many recently developed nanoporous electrodes, such as the A-CNT electrodes described here, can vary over a broad range. The traditional method of evaluating the supercapacitor performance in terms of the gravimetric energy and power densities, in which the only weight of the conductive electrode material is included, will not accurately reflect the device performance when the active material density is very low. For example, due to a very large “empty space” in the ion pathway, a very high power density of 100 kW kg^{-1} was obtained in the supercapacitor with 1% Vf A-CNT electrodes, compared with 50 kW kg^{-1} in the supercapacitor with 40% Vf A-CNT electrodes, because only the weight of the active materials was used here in the calculations. However, if the total electrode weight including both the active materials and the electrolytes, is used to determine the device gravimetric energy and power densities, the supercapacitor with 1% Vf A-CNTs shows a very low gravimetric energy and power density compared with that of the supercapacitor with 40% Vf A-CNTs.

For the supercapacitors with 1% Vf of A-CNTs, the specific gravimetric capacitance will become 4.3 F g^{-1} when the total electrode weight, including both the 1% Vf active material and 99% Vf electrolyte, is

used in the calculation. This is much smaller than 270 F g^{-1} deduced when only the weight of the A-CNTs is included. In contrast, for the 40% Vf A-CNTs, a gravimetric capacitance of 270 F g^{-1} for the active material alone is equivalent to a 139.8 F g^{-1} when all the electrode weight is included. In order to make correction when comparing the electrochemical performance of electrodes with large differences in the active material densities, the *gravimetric efficiency (η)* is introduced here,

$$\eta = M_{act} / M_{eld} \quad (5)$$

where M_{act} and M_{eld} are the weight of the active material and the total weight of the electrode (including both the electrolyte and active material), respectively. Hence, the gravimetric efficiency of the as-grown 1% Vf A-CNTs electrode is only 1.6 %, while that of 40% Vf A-CNTs electrode is 51.8%, when EMI-BF_4/PC is used as the electrolyte in both cases. This is consistent with the data in Figure 3ewhich shows that the electrodes with 40% Vf A-CNTs exhibit a much higher volumetric energy density (75 WhL^{-1}) and power density (>25 kWL^{-1}), compared with that with 1% Vf of A-CNTs.

The 40% Vf A-CNTs supercapacitors also exhibit an excellent cycling life as shown in Figure 3f. The data was acquired over 5000 cycles by repeating the galvanostatic charge/discharge process between 0 and 4 V at a current density of 5 A g^{-1}, which shows an excellent electrochemical stability of the supercapacitors of the ultra-high density A-CNTs with the retention of 98% after 5000 cycles.

To further examine the possible effect of the ultra-high density A-CNTs on the performance of supercapacitor electrodes, the electrochemical impedance spectroscopy (EIS) analysis was performed in the frequency range of 100 kHz to 10 mHz as presented in Figure 4a. Nyquist plots of the electrodes with 1% and 40% Vf A-CNTs show sharp rises at low frequencies and semicircles in the high frequencies. The semicircle behavior is attributed to the charge transfer resistance of the electrodes, while the sharp increase of the imaginary part at low frequencies is due to the capacitive behavior of the electrode. The electrodes with 40% Vf A-CNTs also show much smaller resistance (Z') when normalized with the area of the current collector of the capacitors (Ω cm^{-2}) compared with that of 1% Vf A-CNTs.

For the comparison, the power and energy densities of the electrodes fabricated from the activated carbon with 0.8 mm electrode thickness were characterized, and the electrochemical performances are presented in Figure 4b and Figure 4c. The activated carbon electrodes of 0.8 mm thick exhibit a much lower volumetric energy density and power density (20 WhL^{-1} and 1.1 kWL^{-1}, under 4 V) compared with that of the electrodes with 40% Vf of A-CNTs (75 WhL^{-1} and >25 kW L^{-1} under 4 V). The results indicate the superior electrochemical performance of the ultra-high density A-CNTs electrodes fabricated from the mechanical densification method developed here, which possess the nanomorphology of the aligned ion pathways to achieve fast charge/discharge rate and high power/energy densities.

Figure 4b and Figure 4c reveal that, while increasing the voltage from 3 V to 4 V leads to a large increase in the energy density, from 15 Wh L^{-1} to 75 Wh L^{-1} (30 Wh kg^{-1} 150 Wh kg^{-1}), there is very little increase in the power density. The large increase in the energy density is due to the increase in the specific capacitance of the electrodes with increasing voltage, as shown in Figure 4d. The specific capacitance is 260 F g^{-1} (135 F cm^{-3}) at 4 V. These values are much higher than those reported earlier for the supercapacitors using A-CNTs densified by the liquid collapsing method. On the other hand, the power density also depends on the ESR (see Equation (4)), besides the applied voltage. The results indicate that there is a large increase in the ESR as the peak voltage is increased from 3 V to 4 V, which is consistent

with the results of an earlier study. The transport of mobile ion in ionic devices such as supercapacitors is through diffusion process and drifting process. Diffusion is slower and hence exhibits much higher ESR than drifting process. For supercapacitors with IL/ML electrolytes, an earlier study shows that the capacitance increase at high voltages is caused mainly by the capacitance associated with the diffusion process, which also causes a large increase in ESR at high voltages.

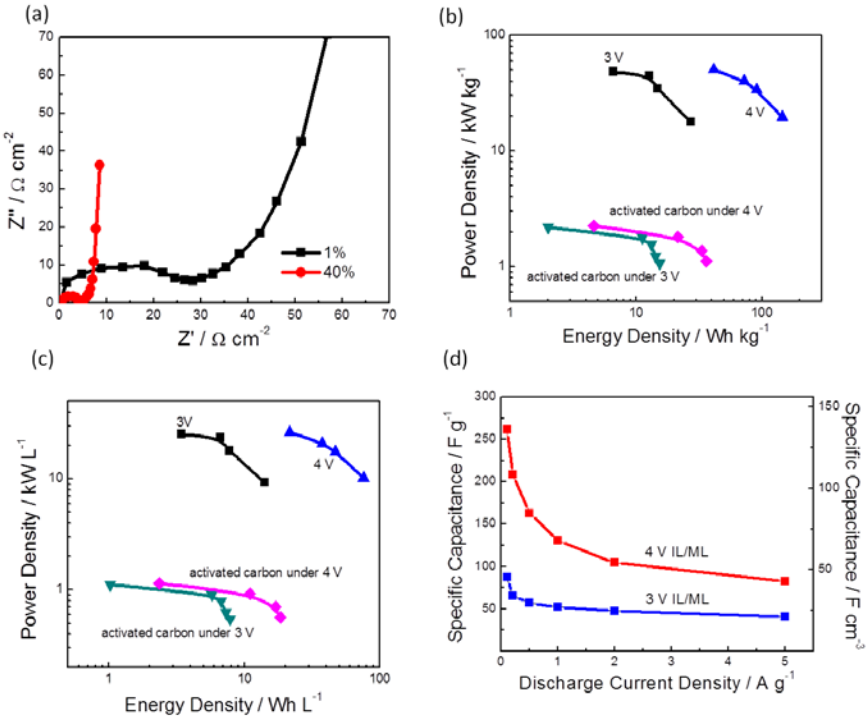

Figure 4. a) Nyquist plots of 1% Vf and 40% Vf A-CNTs supercapacitors in the range of 100 kHz to 10 mHz. b) Gravimetric and c) volumetric Ragone plots of supercapacitors with electrodes of 40% Vf A-CNTs and with electrodes of activated carbon. d) The specific capacitance of supercapacitors with 40%Vf A-CNTs under different discharge current densities.

1.2 High Volumetric Performance Aligned Nano-Porous Graphene-based supercapacitors

Activation of carbon materials is one of the most widely used approaches for increasing the surface area of the carbon electrodes of supercapacitors and hence improve the energy density and power density of the devices. Recently, the activation of microwave exfoliated graphite oxide (MEGO) with KOH was reported by Zhu *et al.* where a surface area of 3100 m^2/g can be achieved and because of the nano-sized pores (bimodal distribution ~ 1 nm and 4 nm), the new activated MEGO (aMEGO) material was named as the 'nano-porous MEGO'. Indeed, this new material with such a high gravimetric surface area as the electrodes for symmetric supercapacitor devices demonstrated very high gravimetric capacitances of 165 and 200 F/g using 1-butyl-3-methyl-imidazolium tetrafluoroborate (BMIM BF_4) and 1-ethyl-3-methyl-imidazolium bis (trifluoromethylsulfonyl) imide (EMIM TFSI) in acetonitrile (AN) as the electrolytes, respectively. Nevertheless, the outstanding high surface area of newly developed electrode materials such as this aMEGO does not necessarily translate to high volumetric performance for a supercapacitor since

their density is typically less than 0.5 g/cm^3. In other words, even though these high surface area materials may exhibit high gravimetric capacitance, and thus high energy or power densities per weight of the active material, their volumetric performance is less compelling. Volumetric performance that requires high density electrode materials is an important metric since technological demands require the design and fabrication of small scale energy storage devices.

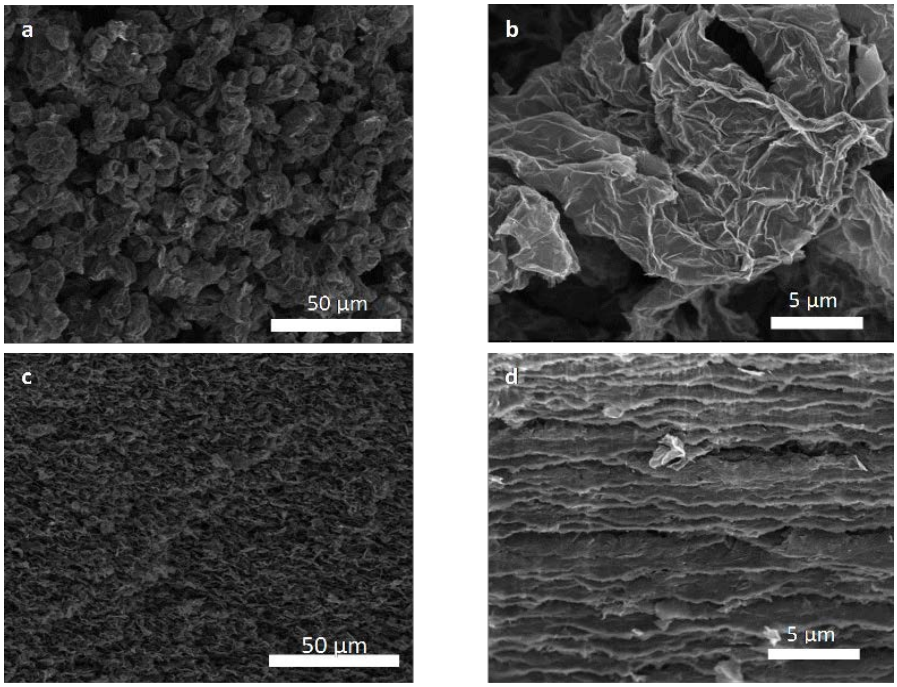

Figure 5. Low and high magnification SEM images of (a) and (b) mechanically densified aMEGO and (c) and (d) aligned aMEGO.

In this program, a vacuum-assisted self-assembly method was developed to densify the aMEGO powder that increased the electrode density to 1.15 g/cm^3, significantly higher than that produced by simple compression. Very high volumetric capacitances of 158 F/cm^3 and 177 F/cm^3 were demonstrated for the aligned aMEGO (A-aMEGO) using BMIM BF_4/AN and EMIM TFSI/AN as the electrolytes, respectively at 1 A/g discharge rate and 3.5 V voltage peak. A minimal reduction in the gravimetric capacitance and energy density was obtained for the A-aMEGO samples showing the enormous improvement in the volumetric values. This is attributed to the highly dense and well-ordered structure of aligned aMEGO sheets, as observed in the SEM images in Figures 5c and 5d, which provides efficient packing of the sheets while preserving the concentration and distribution of nano-sized pores, known to be responsible for charge storage. To our knowledge, the volumetric capacitances obtained here are the highest for any activated carbon-based electrochemical capacitors reported in the literature.

The electrochemical energy storage performance of the A-aMEGO electrodes in BMIM BF_4/AN and EMIM TFSI/AN electrolytes was evaluated using cyclic voltammetry (CV) at different scan rates and voltages. The nearly rectangular CV curves for the electrodes with BMIM BF_4/AN depicting specific volumetric capacitance as a function of the applied voltage is shown in Figure 6. The volumetric capacitance obtained from the CV curve under 5 mV/s scan rate from 0 to 3.5 V was 155 F/cm which is much higher than other results reported to date. This is attributed to much higher density of A-aMEGO electrodes compared to the similar systems. For the electrodes with EMIM TFSI/AN the volumetric capacitance at 5 mV/s was 175 F/cm^3, about three times the value reported for analogous material systems without high force mechanical compression.

To further investigate the capacitive performance of A-aMEGO electrodes, constant current galvanostatic charge/discharge cycling experiments were conducted at different discharge rates and the specific capacitance was calculated from the slope of the discharging curve after the IR voltage drop. The charge/discharge curve for the A-aMEGO electrode with BMIM BF_4/AN as electrolyte is shown in Figure 7a and the data obtained from the curve at 1 A/g along with the reported data for similar studies are presented in Table 1 for comparison. The specific volumetric capacitance at 1 A/g discharge rate and maximum voltage of 3.5 V was 158 F/cm^3 which, consistent with the results from CV curves, is much higher than any reported values (between 50 and 100 F/cm^3) for different types of carbon materials including activated carbon, carbon nanotubes, and even carbide-derived carbon. Similar values were obtained for higher discharge rates of 3, 5 and 10 A g^{-1} where volumetric capacitances of 153, 149 and 147 F/cm^3 were obtained, respectively. The equivalent series resistance (ESR) values were calculated from the IR voltage drop and at 1 A/g discharge rate the ESR values were found to be 14.1 Ω and 10.8 Ω for BMIM BF_4/AN and EMIM TFSI/AN, respectively. This agrees with the higher conductivity of EMIM TFSI compared to that of BMIM BF_4.

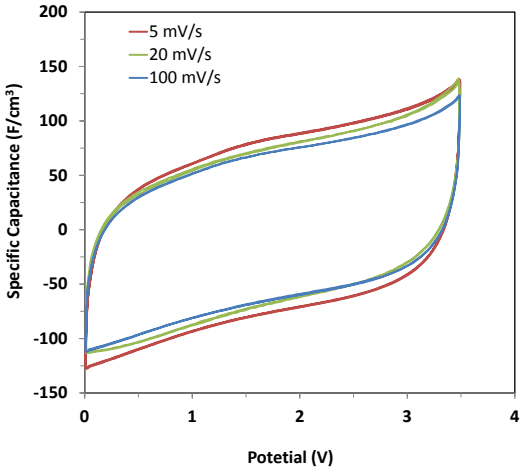

Figure 6. Cyclic voltammetry curves for A-aMEGO samples with BMIM BF_4/AN as electrolyte.

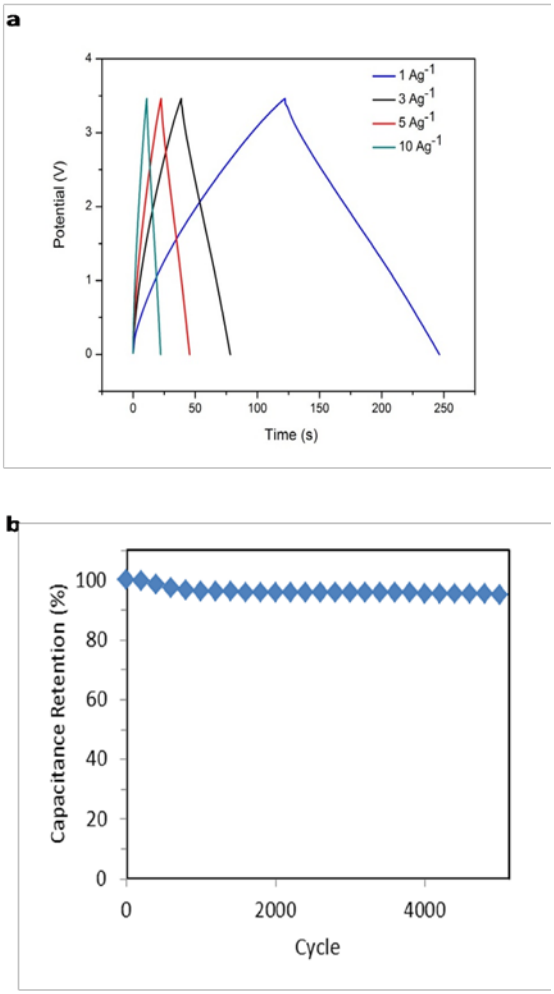

Figure 7. (a) Galvanostatic charge/discharge curve under different constant currents and maximum voltage of 3.5 V for A-aMEGO sample with BMIM BF_4/AN. (b) Capacitance retention test after 5000 cycles for the same sample. Retention of 94% was obtained.

The gravimetric electrochemical performance of electrodes, where only the mass of the active material is considered, has been widely used to compare different active material performance. It is noted that in supercapacitor electrodes, besides the active materials such as porous carbon, there also exist electrolytes. When the densities of the active materials in the electrodes do not differ much (the traditionally carbon based electrodes have density of ~ 0.5 g/cm^3), a comparison of the electrode

performance in terms of per weight of active material alone (gravimetric capacitance, energy density, and power density) is meaningful. On the other hand, for electrodes with large difference of the active material density, a comparison of electrode performance based on per weight or volume of the whole electrode will provide a more realistic picture of the actual device performance. For instance, for the electrodes with the active material density of 0.34 g/cm^3, the electrode density when including for example BMIM BF_4/AN (0.95 g/cm^{3}density) is actually 1.14 g/cm^3. This means that only a small portion of the mass contributes in the energy storage. On the other hand, the density of the A-aMEGO electrode here when including BMIM BF_4/AN is 1.60 g/cm^3. Hence, a specific gravimetric capacitance of 165 F/g for the low density aMEGO using the active material alone, as reported earlier, translates to a gravimetric capacitance of 49.2 F/g when the total electrode weight, including both the active material and electrolyte, is used. In contrast, for the A-aMEGO electrode which has an active material density of 1.15 g/cm^3, a gravimetric capacitance of 154 F/g for the active material alone is equivalent to a 110.7 F/g when all the electrode mass is included. In this paper, the gravimetric values of active material (ACT) and that of electrode (ELD) are used to distinguish between these two gravimetric values of an electrode. As shown in Table 1, there is a close correlation between the specific gravimetric performance in terms of the whole electrode weight and the specific volumetric performance. The results also indicate the importance of the volumetric performance of a supercapacitor as a more meaningful device parameter for practical applications rather than the gravimetric performance in terms of the active material only.

As shown in Table 1, the gravimetric results of ACT for A-aMEGO samples are slightly lower than the reported values for similar electrode systems with lower densities. This trend indicates that the presence of the macro- sized -pores in the low density aMEGO electrodes facilitates the ion transport so that the gravimetric accessible surface area per active material for a given discharge rate is higher than the high density A-aMEGO electrodes prepared here, which is comprehensible. Compared to the low density aMEGO or mechanical compressed samples, the average pore size is reduced in the A-aMEGO electrodes which is a result of efficient packing of graphene sheets during the self-assembly process. This efficient packing results in increased bulk density of the electrode and hence the volumetric capacitance values for A-aMEGO samples are significantly higher than the reported values for carbon-based electrodes in the literature.

The device performance in long term cycling was investigated at a rate of 5 A/g and maximum voltage of 3.5 V for 5000 cycles. The specific capacitance retention as a function of cycle number for the electrodes with BMIM BF_4/AN is presented in Figure 7b. After a small decrease of specific capacitance in the first 1000 cycles, its retention value stayed nearly constant at 94% during 5000 cycles. This again confirms that there are no electrochemical reactions involved in the capacitance process and also the pore accessibility for the aligned activated MEGO does not change by cycling.

Table 1. Comparison on gravimetric and volumetric performance of A-aMEGO samples with lower density aMEGO electrodes (the thickness of each electrode is 0.1 mm)

Sample	*Active Material Density (g/cm^3)*	*Gravimetric Capacitance at 1 Ag^{-1} (per active material weight) (F/g)*	*Gravimetric Capacitance at 1 Ag^{-1} (per whole electrode weight) (F/g)*	*Volumetric Capacitance at 1 Ag^{-1} (per active material weight) (F/cm^3)*	*Gravimetric Energy Density(per active material weight) (Wh/kg)*	*Gravimetric Energy Density (per whole electrode weight) (Wh/kg)*	*Volumetric Energy Density (Wh/l)*	*Power Density (W/l)*
A-aMEGO/ BMIM BF_4/AN	1.15	137	99	158	58	42	67	119
A-aMEGO/ EMIM TFSI/AN	1.15	154	104	177	66	45	75	130
aMEGO/ BMIM BF_4/AN	0.34	165	49	56	70	21	24	85
Compressed aMEGO/ BMIM BF_4/AN	0.75	147	70	110	63	34	48	17

Energy density and power density as two governing metrics of supercapacitors were investigated using the values obtained from galvanostatic experiments. The volumetric energy density for the A-aMEGO electrodes with BMIM BF_4/AN from the data at 1 A/g was 67.0 Wh/l. For samples with EMIM TFSI/AN the volumetric energy density was found to be 75.3 Wh/l. Increasing the discharge rate did not considerably influence the performance of the device in terms of energy density. The volumetric energy density values were found to be 65.1 Whl^{-1} and 63.2 Wh/lfor electrodes with BMIM BF_4/AN and 72.9 Wh/l and 70.9 Wh/l for samples with EMIM TFSI/AN at 3 Ag^{-1} and 5 Ag^{-1} discharge rates, respectively.

The power density for these samples was calculated from the IR drop. Figure 8a compares the volumetric and Figure 8b the traditional gravimetric values (per active material mass only) for power and energy densities. As shown in the Ragone plot in Figure 8a, the volumetric power density values from the data at 1 A/g rate were 119 kW/l for the electrodes with BMIM BF_4/AN and 130 kW/l for the electrodes with EMIM TFSI/AN. These values are remarkably large for supercapacitors based on graphene/ionic liquid combinations and it can be attributed to the dense morphology while maintaining the ordered pathway for ion propagation in the A-aMEGO supercapacitors.

These high volumetric energy and power densities make high bulk density A-aMEGO electrodes suitable candidates for practical large scale applications where a greater amount of this material can be included inside packaged supercapacitor devices. A-aMEGO samples exhibit the highest power density per total electrode weight compared to the others reported in the literature.

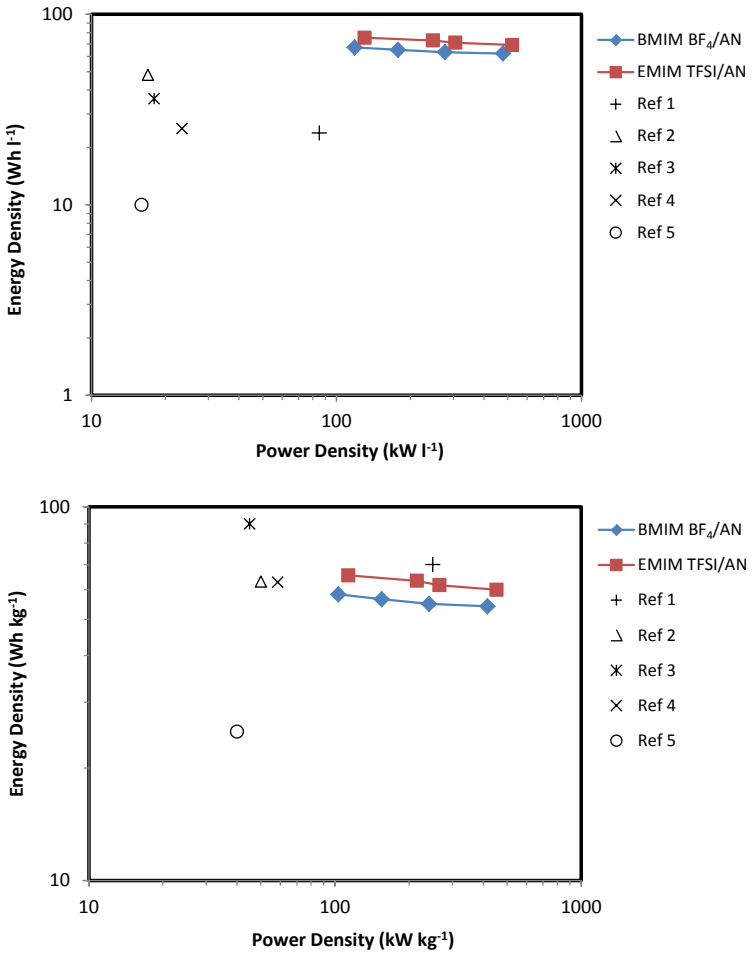

Figure 8. Ragone plot for A-aMEGO samples along with the highest reported values for graphene/ionic liquid combinations under similar voltage and discharge current values. (a) Volumetric values and (b) gravimetric values (per active material weight).

References: 1. Y. Zhu et al., *Science* **2011**, *332*, 1538. 2. S. Murali et al., *Nano Energy* **2013**, DOI 10.1016/j.nanoen.2013.01.007. 3. C. Liu et al., *Nano Lett.* **2010**, *10*, 4863. 4. Q. Cheng et al., *Phys. Chem. Chem. Phys.* **2011**, *13*, 17615. 5. Y. Zhu et al., *Nature Communications* **2012**, *3*, Article number: 1225.

Understanding of the ion diffusion in the A-aMEGO electrodes was obtained by conducting electrochemical impedance spectroscopy measurements in the frequency range of 10 mHz to 1 MHz and using DC bias voltages of 2.5 and 3.5 V to evaluate the impedance dependency on voltage. Figure 9a shows the Nyquist plot for the electrodes containing BMIM BF_4/AN and the inset in the figure shows the high frequency region of the Nyquist plot. Regardless of the bias voltage, Nyquist plot is similar in shape for all three measurements and all the plots show a steep rise in the imaginary axis at low frequency which is a characteristic of the capacitive behavior (the imaginary part of the electric impedance is much larger than the real part of the electric impedance). At high frequency region, similar shapes with a slight increase in the high frequency resistance with the bias voltage were observed, indicating an increased resistive behavior of the electrode with the bias voltage. In the middle frequency range of the Nyquist plot ion migration in the electrode can be investigated and the effect of electrode porosity and thickness on this

migration can be studied. Additionally, the imaginary part of the impedance (in absolute value) decreases with the DC bias voltage. This result indicates that the capacitance value increases with the DC bias voltage, and this increase can be interpreted as being due to the increase in the dielectric constant of the electrolyte or to the decrease in the charge separation distance induced by applying bias potential. This confirms that the charge storage is nearly pure double layer and no evident electrochemical reaction takes place under 3.5 V DC bias voltage.

The real part of capacitances (C') as a function of frequency for the A-aMEGO electrodes are presented in Figure 9b. The capacitance value at low frequencies for the electrodes containing EMIM TFSI/AN was higher compared to that with BMIM BF_4/AN, which is consistent with the slightly higher capacitance and energy density obtained from galvanostatic experiments for this sample.

In summary, aligned nano-porous aMEGO electrodes were fabricated using a vacuum-assisted self-assembly process followed by slow infiltration of PTFE binders which led to very high bulk density of 1.15 g/cm^3. The experimental results revealed the near optimal nano-morphology of the electrodes which eliminates the micron-sized pores (presented in the carbon based electrodes using traditional fabrication methods and do not contribute to the energy storage, therefore reduce the volumetric energy density of the devices) while maintaining high nano-sized pores that are responsible for the formation of electric double layer and energy storage. Very high volumetric capacitance of 158 Fcm^{-3} for the A-aMEGO with BMIM BF_4/AN and 177 F/cm^3 for the sample with EMIM TFSI/AN as electrolyte were obtained. The gravimetric capacitance in terms of the mass of the active material was 137 F/g for the A-aMEGO with BMIM BF_4/AN and 154 F/gfor sample with EMIM TFSI/AN as electrolyte, which are slightly lower than that (165 F/g and 200 F/g for the two electrolytes, respectively) obtained from the aMEGO electrodes using the traditional fabrication method. *The A-aMEGO electrodes thus fabricated exhibited very high volumetric energy density of 67.0 Wh/L and 75.3 Wh/L and power density of 490 kW/L and 510 kW/L using BMIM BF_4/AN and EMIM TFSI/AN, respectively*. Exceptionally high volumetric performance of the A-aMEGO electrodes introduces a realistic energy storage device configuration to meet various technological demands.

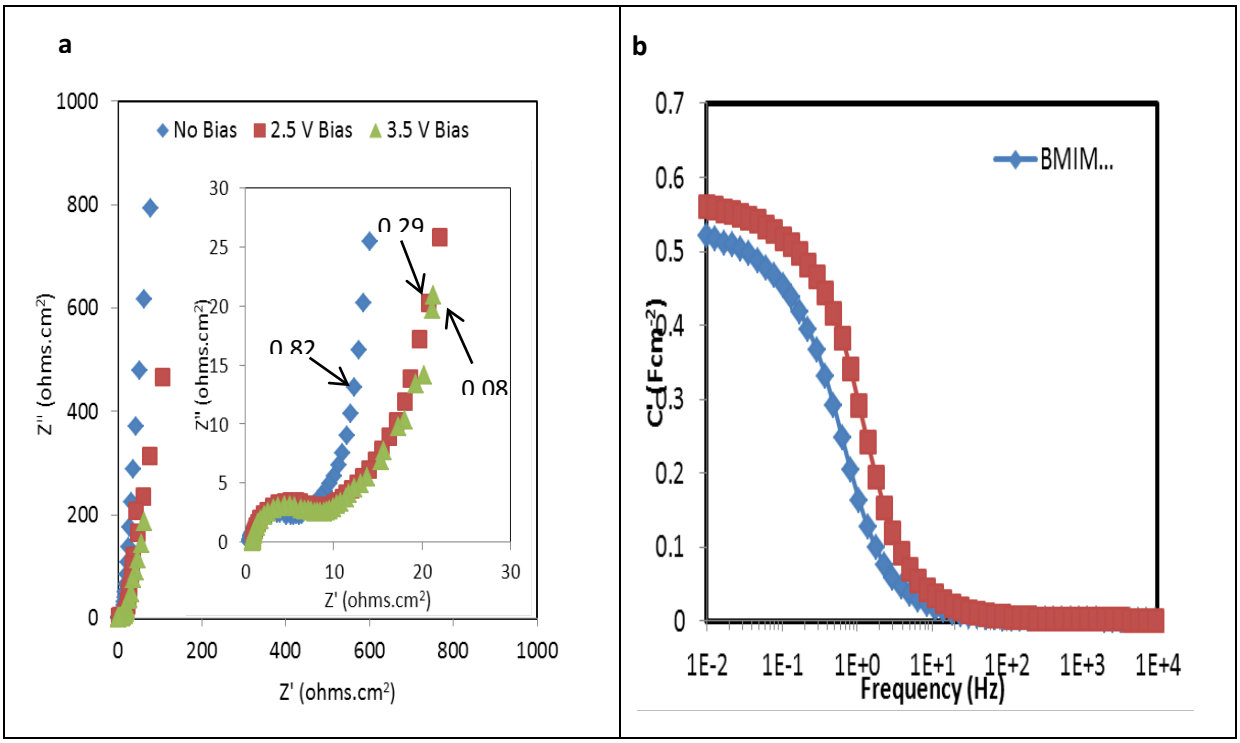

Figure 9. (a) Nyquist plot for A-aMEGO samples at 10 mHz to 1 MHz frequency range and no DC potential, 2.5 V and 3.5 V DC bias. The inset is the data for high frequency region. Arrows show the frequency where $Z' = Z''$. (b) Real part of capacitance as a function of frequency, indicative of the high dependent capacitance at low frequencies.

1.3 Highly Efficient Hybrid Supercapacitor Materials from Conformally Coated Aligned Carbon Nanotubes with Poly (3,4-ethylenedioxythiophene)

Due to their high surface area and conductivity, carbon based materials such as activated carbon (AC) and carbon nanotubes (CNTs) have been extensively investigated as active electrode materials for supercapacitors. Carbon nanotubes are especially attractive for their superior properties compared to other materials. Nevertheless, carbon nanotubes suffer from the fact that the charge accumulation takes place only on the surface, limiting the specific capacitance magnitudes. To address this limitation, conducting polymers (CPs) such as polyaniline (PANI), polypyrrole (PPy) and poly (3,4-ethylenedioxythiophene) (PEDOT) have been used to conformally coat carbon nanotubes since in CPs the entire mass and volume of the polymer is involved in the charge storage process, resulting in extremely high capacitance values.

Despite this improved charge storage capability, the traditionally CP-coated randomly packed CNTs are not ideal electrode materials for supercapacitors. For example, the ion transport path in these electrodes is tortuous that results in high time constant values for mobile ion transport in these porous electrodes (Figure 10a) and hence reduced power density. In addition, the mechanical failure of CPs, caused by the large volume change during the charge/discharge process of CP, filling the gaps between CNTs, still causes large reduction of capacitance at long cycle operation. Perhaps the most effective approach to address these problems is the alignment of the CNTs where the ordered nano-morphology facilitates the ion transport by providing highly aligned ion transport pathways between the current collectors and the

capacitor separator (Figures 10a and 10b), resulting in higher power density. This continuous ionic conduction pathway also significantly reduces the effect of the large volume changes of CPs during charge cycles on the electronic conductivity (Figure 10b) and improves the cycle life of the capacitors, as will be shown in this paper.

In contrast to other methods of CP coating on CNTs reported in the literature, which result in non-uniform coating of CPs on randomly packed CNTs, the o-CVD method is shown to uniformly coat A-CNT of very high aspect ratio (here 200 mm long *vs.* 8 nm diameter of CNT) with PEDOT at all inter-CNT spacing, as revealed by the TEM image in Figure 10c. Consequently, this o-CVD process preserves the aligned nano-morphology of A-CNTs (Figure 10b).

In order to evaluate the amount of the coated PEDOT on A-CNTs, thermo-gravimetric analysis (TGA) was performed on the electrode materials. As shown in Figure 10d, the pristine A-CNT does not show any substantial degradation up to 800^0C. However, PEDOT-coated electrode exhibited a two-stage weight loss process starting at about 270^0C. The weight residue for this sample was 70 wt % which is attributed to the remaining A-CNTs. Therefore, the PEDOT/A-CNTs electrode fabricated contains 30 wt % of PEDOT. Considering the density of the two materials, this translates into an 8-10 nm thick PEDOT conformally coated on A-CNT.

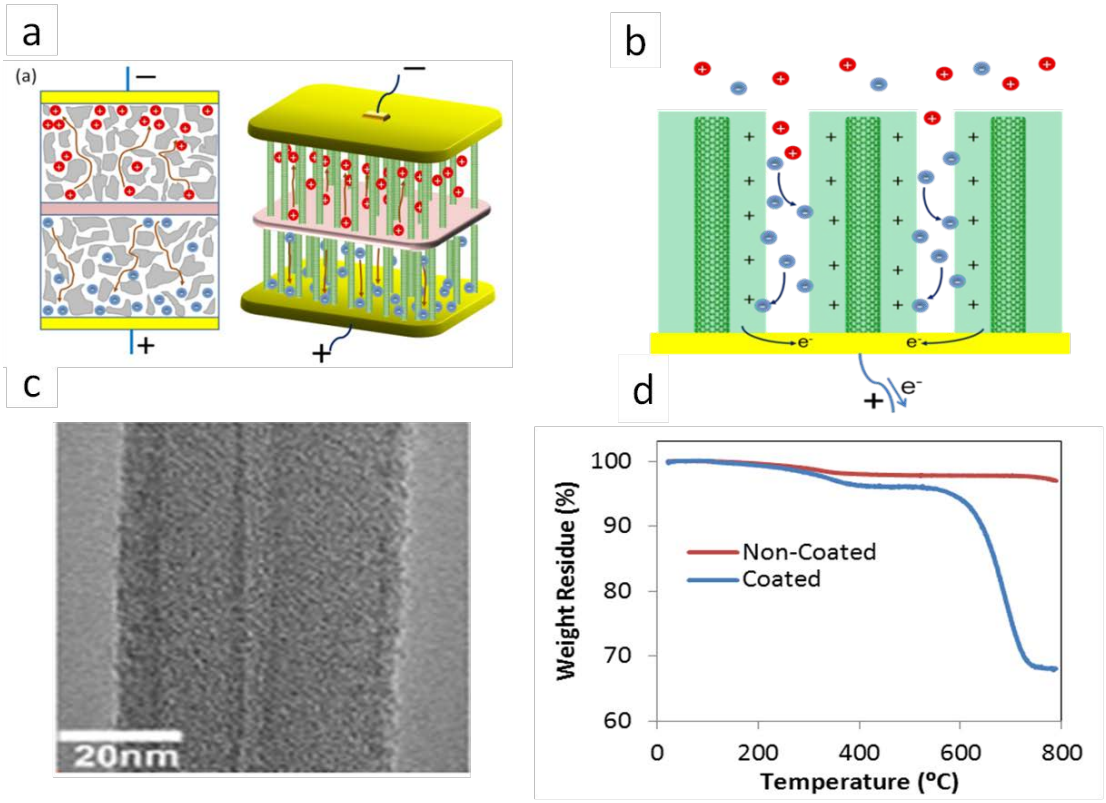

Figure 10. (**a**) Schematic comparison of the tortuous ion transport paths in nanoporous electrodes formed, for example, from activated carbons (left), and parallel ion pathways in the A-CNTs (right). (**b**) Schematic representation of CP coated A-CNT used as supercapacitor electrode. Cations and anions along with electrons and holes are shown in the figure. (**c**) TEM image of A-CNT conformally coated with PEDOT.

The contrast in the image shows the uniform coating of PEDOT on A-CNT. (**d**) TGA plots for the coated and non-coated samples.

The electrochemical performance of the PEDOT/A-CNT electrodes was evaluated by cyclic voltammetry (CV), galvanostatic charge/discharge cycling and electrochemical impedance spectroscopy (EIS) using a two electrode cell configuration. The CV curves for non-coated A-CNTs (1% and 5% V_f) as well as the PEDOT/A-CNT (1% and 5% V_f) electrodes over the voltage range from 0 to 2 V under 100 mV/s scan rate are shown in Figure 11. Both the PEDOT coated and non-coated electrodes show nearly rectangular CV curves which are indications of the highly capacitive nature of the electrodes with fast and reversible charge/discharge process. As expected, the higher specific capacitances of the PEDOT coated A-CNTs electrodes, due to the higher charge storage capability of PEDOT, manifest higher current density than those of pristine A-CNTs.

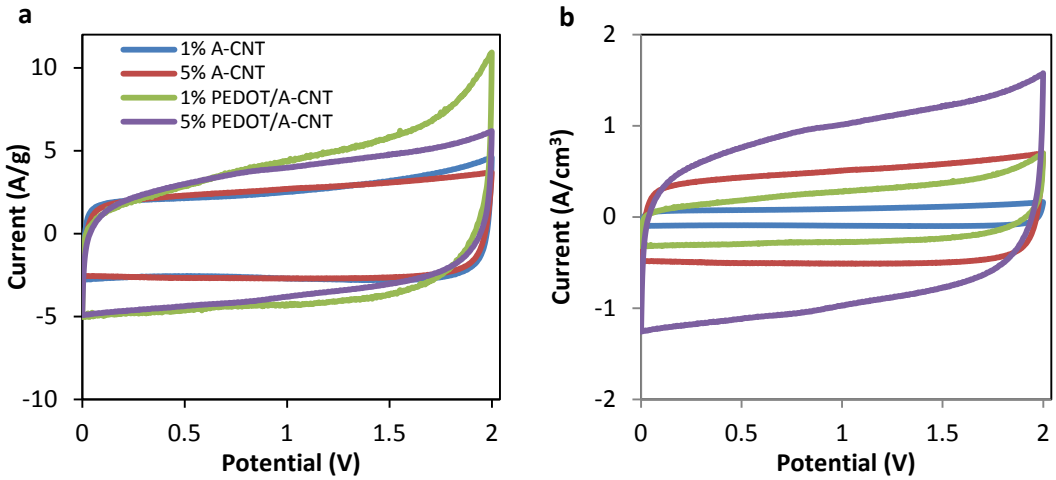

Figure 11. Cyclic voltammetry curves for the pure A-CNT and PEDOT/A-CNT electrodes at 100 mV/s scan rate. (**a**) Gravimetric and (**b**) volumetric current density as a function of applied voltage.

Further investigation of the capacitance for PEDOT/A-CNT samples was performed by the discharge curves of the galvanostatic charge/discharge test and the cycles at 0.5 A/g are shown in Figure 12a. For the non-coated samples, an electric double layer charge storage mechanism is conceivable, whereas for the coated samples the nearly symmetric and linear charge/discharge characteristics reveal a rapid I-V response and a reversible electrochemical reaction, implying an excellent capacitive behavior for the PEDOT/A-CNTs based electrodes. The gravimetric and volumetric capacitance values obtained from galvanostatic cycles at different scan rates are compared in Figures 12b and 12c, respectively. Similar to the values obtained from the CV curves, the PEDOT coating significantly enhances the capacitance values and once combined with the mechanical densification of the A-CNT forests, a very high volumetric capacitance value of 44.2 F/cm^3 was obtained for 5% PEDOT/A-CNTs composite electrode at 0.5 A/g, which is substantially high compared to the similar systems (see Figure 12c). A high volumetric performance is attractive since most practical energy storage devices require compact device size. Moreover, Figure 12b reveals that the densification of the electrodes from 1% V_f to 5% V_f A-CNTs does not cause marked change of the specific gravimetric capacitance, indicating that the mechanical

densification process employed here can preserve the nano-morphology of the fast ion transport pathways of the A-CNTs. Therefore, conformal coating combined with the densification significantly improves the capacitive characteristic of A-CNT and results in a useful electrode material for electrochemical charge storage applications.

The performance of PEDOT/A-CNT electrodes in long term charge/discharge cycles was evaluated by galvanostatic test for capacitance retention at 10 A/g during 1000 cycles (Figure12d). The capacitance retention for PEDOT/A-CNT electrode under maximum voltage of 2 V was 90%, whereas the retention for random PEDOT/CNT under the same condition was found to be 73%. In the randomly packed CNT networks, CPs are coated non-uniformly and there are junctions of CPs bridging in between the CNTs. During the charge/discharge cycling these CP bridges will experience large mechanical deformation, which eventually leads to mechanical failure and disrupts the electronic conduction of the CNT network, resulting in the deteriorated capacitance. In contrast, in the PEDOT/A-CNTs electrodes, the A-CNTs form continuous electronic conduction paths as schematically illustrated in Figure 10a and the mechanical failure of the CP nano-coating layers, even if it occurs, will not have much effect on the electronic conduction process of the electrodes. Hence, the PEDOT/A-CNT electrodes exhibit much robust mechanical stability and high retention of the capacitance, compared with the electrodes of the CP deposited on randomly packed CNT networks. Figure 12d also reveals that the mechanical failure of CPs also occurs in the PEDOT nano-layers which cause reduction of the capacitance with the charge/discharge cycles, when compared with the non-coated A-CNTs, which show a 99% capacitance retention after 1000 cycles.

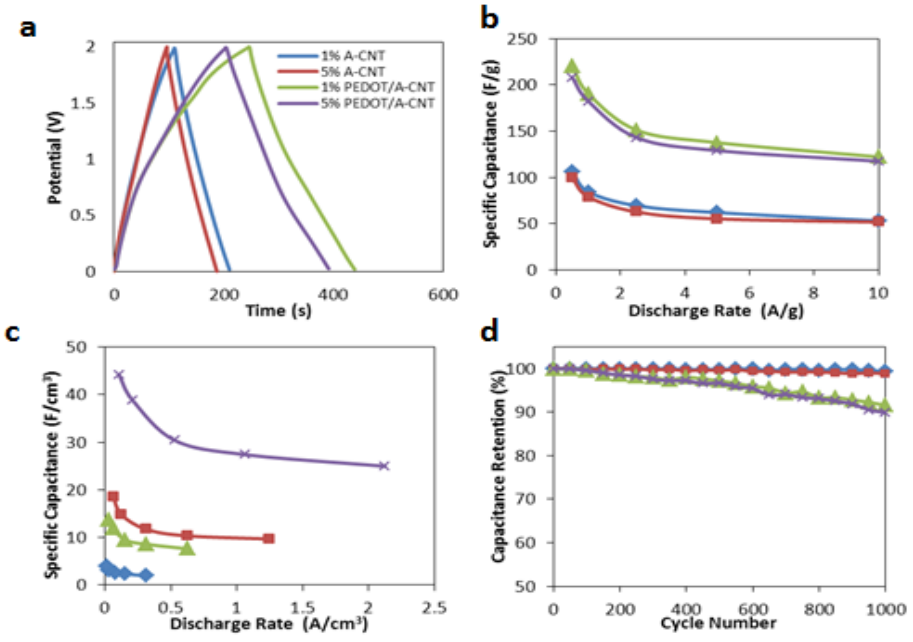

Figure 12. (**a**) Galvanostatic charge/discharge curves for A-CNT electrodes at 0.5 A/g discharge rate. (**b**) Gravimetric and (**c**) volumetric specific capacitance obtained from galvanostatic cycles as functions of discharge rate. (**d**) Capacitance retention for the A-CNT electrodes during 1000 charge/discharge cycles at 10 A/g discharge rate.

Energy and power densities as governing metrics in electrochemical capacitors were evaluated using the data obtained from galvanostatic cycles. The volumetric Ragone plot for the A-CNT electrodes is shown in Table 2. The volumetric energy density values for non-coated and coated (5%) electrodes at 0.5 A/g discharge rate were found to be 2.49 Wh/l and 11.8 Wh/l, respectively. This is comprehensible since the PEDOT/A-CNTs electrodes exhibit significantly higher specific capacitance values. Similar trend is observed for the non-densified electrodes where the coated A-CNTs show energy density of 1.86 Wh/l compared to 0.54 Wh/l for the non-coated electrodes. These specific energy density values are significantly high compared to other PEDOT coated CNTs composites reported earlier and this is a direct result of conformal coating and higher density of coated A-CNTs electrodes investigated in this study. Similar to the energy density, the power density for the densified PEDOT/A-CNT electrodes is significantly higher than that from the non-densified A-CNTs electrodes. For instance, the volumetric power density for the PEDOT/A-CNT electrodes (5% V_f) from the data at 10 A/g is 34.0 kW/l, whereas the value for the non-coated and non-densified sample is only 4.7 kW/l. Gravimetric power densities of the non-densified electrodes are slightly higher than those of densified electrodes due to the slight increase in the ion transport resistance in the densified electrodes.

The A-CNT based electrodes were further characterized using impedance measurements. The imaginary *vs*. the real component of the total impedance for different electrodes are plotted in the Nyquist plot of Figure 13a. At the high frequency region (the inset in Figure 13a), all the electrode materials exhibit a semicircle, which is typical for electrochemical systems, with a small radius of curvature indicating low resistance to charge transfer for all the electrodes. Nevertheless, the radius of this semicircle is larger for the non-coated samples compared to the coated samples which is due to the lesser charge transfer (or the lower capacitance) of the non-coated samples. In other words, the relative lower resistance for the PEDOT/A-CNTs reveals that the core-shell morphology of these electrodes promotes the electrolyte ion insertion/de-insertion process into/from the CP coating layer. This, in turn, results in the larger amount of ions stored in the PEDOT coated electrodes (higher capacitance) which are consistent with the results from other experiments.

Table 2. Volumetric energy and power densities of cells based on A-CNTs electrodes and PEDOT/A-CNTs electrodes.

Sample	**Energy Density (Wh/L)**	**Power Density (kW/L)**
1% A-CNT	0.54	4.7
5% A-CNT	2.49	14.1
1% PEDOT/A-CNT	1.86	9.6
5% PEDOT/A-CNT	11.8	34.0

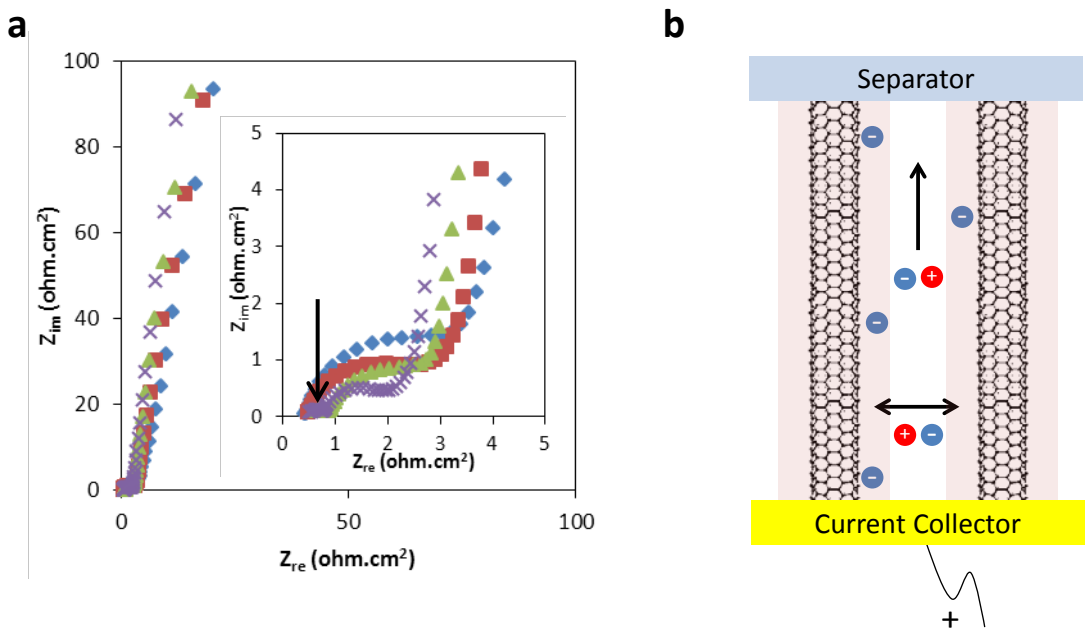

Figure 13. (**a**) Nyquist plot for the A-CNT based electrodes with the high frequency region as the inset. (**b**) Schematic of the two distinct ion transport mechanisms in PEDOT/A-CNT electrodes, i.e. ion transport between aligned CNTs and ion transport through PEDOT layer.

Another interesting trend is that the coated electrodes exhibit an extra semicircle in the higher frequency region, as indicated by the arrow in the inset of Figure 13a, that is significantly smaller than the main semicircle from charge transfer resistance. It is speculated that this additional depressed semicircle can be related to the ion diffusion resistance inside PEDOT as well as the contact resistance between the A-CNT and PEDOT. As shown in Figure 13b, there are two distinct ion migration processes, i.e. the ion migration through A-CNT aligned ion pathway and the ion insertion/de-insertion into/from PEDOT later. The smaller semicircles in the coated samples (that appears at higher frequencies) imply that the second process is faster (smaller time constant) than the first process. The much smaller time constant for the ions insertion/de-insertion in the PEDOT nano-layer, compared with the much longer time constant of the ion transport time through the ion pathways between the A-CNTs, as revealed in Figure 13a, does not affect the overall supercapacitor operation frequency. The combined effect makes the conformally coated PEDOT/A-CNTs electrodes extremely advantageous compared with other electrodes. Also, since these small semicircles occur at high frequencies (> 10 kHz), it can also be concluded that these resistive mechanisms do not influence the capacitive behavior of the PEDOT/A-CNT electrodes.

At the low frequency region all the electrode materials exhibit nearly vertical lines that are indications of near ideal capacitive behavior. Consistent with the data from CV and galvanostatic experiments, the densified PEDOT/A-CNTs electrodes show the steepest increase in the imaginary impedance which is related to the highest capacitive behavior for this electrode. In addition, it is evident that the 45^0 Warburg regions for all the electrode materials are extremely small signifying fast ion re-arrangement/kinetics of the electrolyte ions in these electrodes owing to the aligned morphology of the A-CNTs .

In summary, highly aligned carbon nanotubes forest was conformally coated by PEDOT through an o-CVD process, which led to a uniform layer of the PEDOT coated on the CNT surface along the whole

length, which was then densified using a mechanical densification process to increase the volume fraction of the A-CNTs from 1% (as prepared) to 5%. This newly prepared material was used as the electrode for supercapacitor without the aid of a binder and using a 3M solution of EMI-BF_4 in PC as the electrolyte. Electrochemical analysis including CV and galvanostatic tests revealed that the PEDOT coated A-CNTs exhibit a significant improvement in the capacitance and energy and power density values of the electrodes, related to the significantly increased charge storage capability, fast and reversible charge/discharge process and fast ion propagation in these electrode materials. On the other hand, A-CNT acted as a robust backbone for PEDOT and hence improved its cycle life during charge/discharge process which is reflected on the life cycle data for the A-CNT based electrodes. The aligned nano-morphology of the A-CNT arrays significantly improved the life cycle as well as the electrochemical performance of the electrodes as a result of facilitated ion propagation.

1.4 Conducting Polymer and Aligned Carbon Nanotubes As Composite Electrodes for Supercapacitors – Material Study.

Recently, conformal nm-scale coatins of CP have been investigated as pseudocapacitor electrodes. Compared with EDLC whose working mechanism is based on charge storing on the surface of the porous electrode (e.g., A-CNTs), the CP provides a volume for the redox reaction and energy storage, resulting in a superior specific energy density. However, CP electrodes are well known for relatively poor cycle life attributed to the large volume change and consequent polymer degradation during the charge/discharge process and hence are not suitable for supercapacitor electrodes when used alone. Hence, in this work, composite electrodes combining conformal PEDOT and A-CNTs were fabricated. As shown in Figure 14 (top), the A-CNTs provide the parallel pathways to enhance the rate of ion transport, reduce the electric resistance and improve the ion accessibility under higher current densities. The A-CNTs also provide a porous scaffold to deposit PEDOT via CVD. To fabricate PEDOT/ A-CNT electrodes, the conducting polymer was conformally deposited on 250μm long A-CNTs using oCVD, varying thickness from few to ten nm by controlling deoposition and polymerization times.

Electron microscopy and thermogravimetric analysis (TGA) were used to characterize the morphology of the PEDOT on the A-CNTs as a function of oCVD deposition time. SEM imaging (Figure 15) confirms that the aligned morphology is maintained and that the ultrathin (up to10 nm) vapor deposited polymers are smooth and continuously cover the entire surface of the aligned nanotubes. Thickness measurements via TEM (done on at least 10 individual CNT from every specimen) were compared to the thickness calculated from TGA, showing agreement between both techniques within fidelity of the measurements.

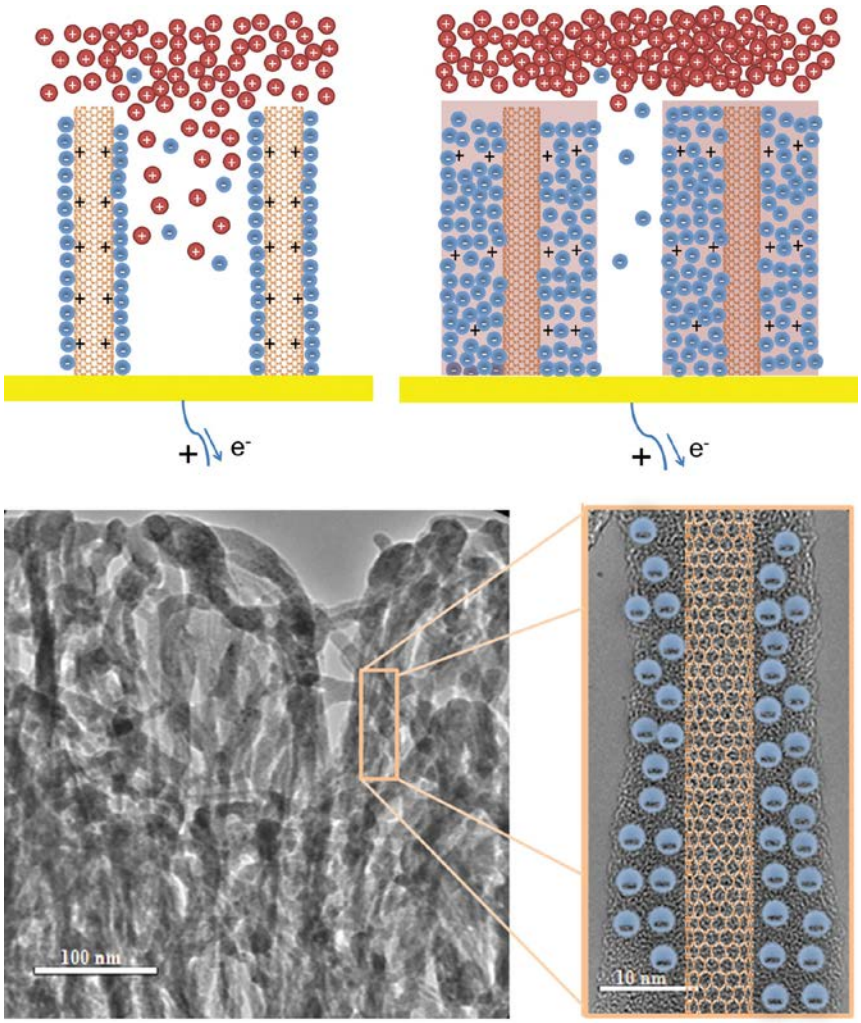

Figure 14. Aligned CNT, conformally coated with PEDOT CP for ion storage. Top: Illustration of uncoated (left) vs. CP-coated A-CNT electrode (right). Charge is stored throughout the polymer volume, as opposed to on the CNT surface in the uncoated electrode. Bottom: HR-TEMs of the CP-coated A-CNT electrode structure. Inset shows 10 nm of PEDOT coating on a CNT (illustrated for emphasis) with illustration of the ions stored volumetrically in the PEDOT CP.

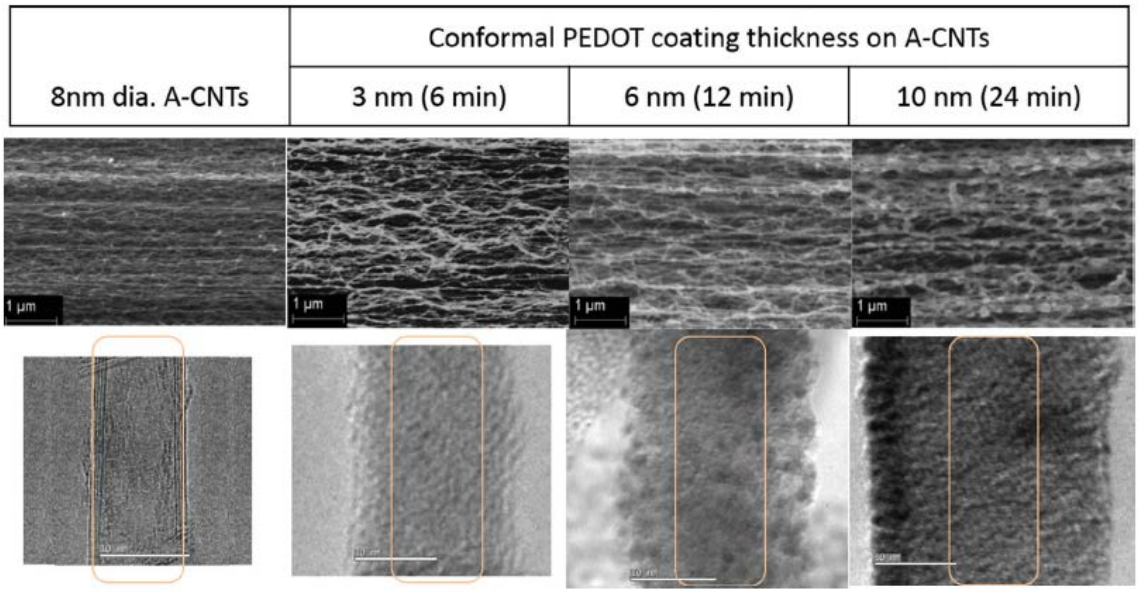

Figure 15. SEM (top) and TEM (bottom) of varying CP thickness coating on A-CNT. All the scale-bars in the TEM images are 10nm and the size and location of the CNT outer wall is indicated in the CP-coated images.

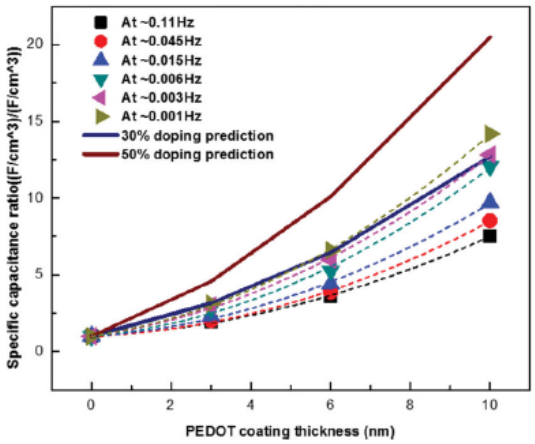

Figure 16. Relative contribution to specific capacitance from PEDOT coating as a function of CP thickness and frequency. Predictions show capacitance for 30% and 50% doping, e.g., in 50% doping every 2 nd site is available for ion/charge storage. Specifi c capacitance of the uncoated A-CNT is 6.54 F/cm 3 utilizing total electrode volume.

The quality of the CP films was assessed by quantifiying charge carrier density active in the films, compared to the expectation of the same polymer in thin-film on flat substrates. Using the capacitance relation C = Q/V, and assuming 30–50% of the sites are doped and active, the theoretical PEDOT contribution to capacitance was calculated. Q is defined as the doping charge on the polymer, and is calculated as 1 electron (1.6E-19 Coulomb) per doped molecule. A working voltage to the electrochemical window of the electrode (2V) was also assumed. The repeat unit on the polymer has a MW of 142 g/mol

and a specific gravity of 1.7 g/cm 3, and the volume of the polymer is calculated as a cylinder of the coating thickness around every individual CNT. Assuming a uniform conformal coating of 5% V f A-CNT (in a 0.45 ×0.45 cm^2 area) the measured and predicted volumetric specific capacitances (normalized to the electrode volume) of all cells under various scan rates is shown in Figure 16.

As seen in Figure 16, volumetric specific capacitance (SC) increases with PEDOT coating thickness on A-CNTs. More importantly, the experimental trend is in agreement with the theoretical calculations, implying that even after mechanical densification of the CP/A-CNT from 1% V f to 5% Vf, the quality of the deposited film is preserved. Also seen is the effect of scan rate on SC: in all the electrodes, lower scan rate results in higher SC, and the difference is only slightly more pronounced for thicker PEDOT coatings. The results demonstrate that at low scan rates (typical supercapacitor charge/discharge time is ~50 second, corresponding to 0.02 Hz or lower frequencies) nearly all of the active sites are available and participate in the charge/discharge process, contributing SC through the entire thickness. The fact that the experimental data follows the 30% doping prediction for the entire thickness range suggests that this dependence is caused by the mobile ions slow diffusion into and out of the A-CNT electrode (250 μm thickness), and not by the faster travel through the relatively thin (3–10 nm) CP coating. As a result, 10nm PEDOT coated A-CNT electrode can store **10 times more charge per volume, and 50% more charge per weight**, than their uncoated equivalent.

However, the increased PEDOT coating thickness decreases the Coulombic efficiency (see Figure 17). When the scan rate is suitably low (10 mV/s) to allow the pseudocapacitor time to store and release charge, all cells, with CP coating up to 10nm, exhibit nearly ideal capacitive behavior (so that the Coulombic efficiency shows only a slight decrease, and is overall very close to 100%). Moreover, and as a further support of the attribution of the energy loss to the slower diffusion of ions in the electrode, at the slow scan rate the change of Coulombic efficiency with thickness shows the least decay (Figure 17 b).

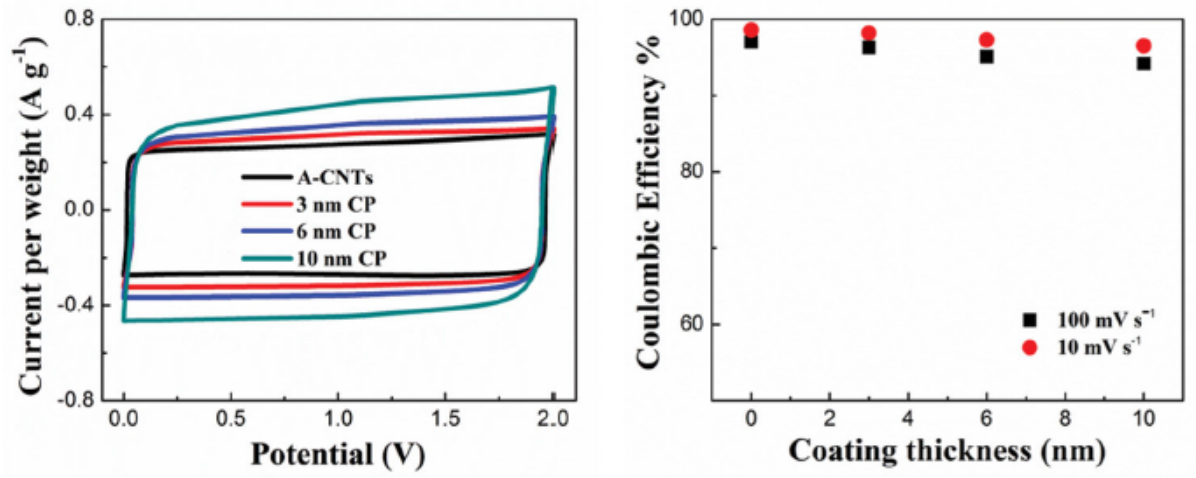

Figure 17. Effects of voltage scan rate on capacitance performance of cells with and without CP coating in 2 M BMI-BF 4 /PC under the scan rates of 100 mV /s and 10 mV /s. Left: CV curve of cells with different electrodes at a scan rate of 10 mV/s . Note the slight bump at 1V in the charge curve, absent from the discharge curve, which is attributed to PEDOT reduction. Right: Coulombic efficiencies as a function of coating thickness at different scan rates.

Increasing the thickness of the conformal PEDOT, and thus increasing the specific capacitance, C, systematically increases both the observed energy and power density (see Figure 18. The energy density for the thickest PEDOT film utilized in this work (10 nm) is enhanced 8X-10X at a fixed current density as compared to uncoated A-CNTs on a volumetric basis. Both energy and power density improvement of more than an order of magnitude are achieved as compared to industry-standard activated carbon. In the range considered, diffusion of ions in the CP films is not rate limiting, suggesting that further increasing PEDOT thickness while avoiding keyhole formation (*i.e.*, PEDOT blocking the ion channels), is a viable route towards increasing electrode performance even further.

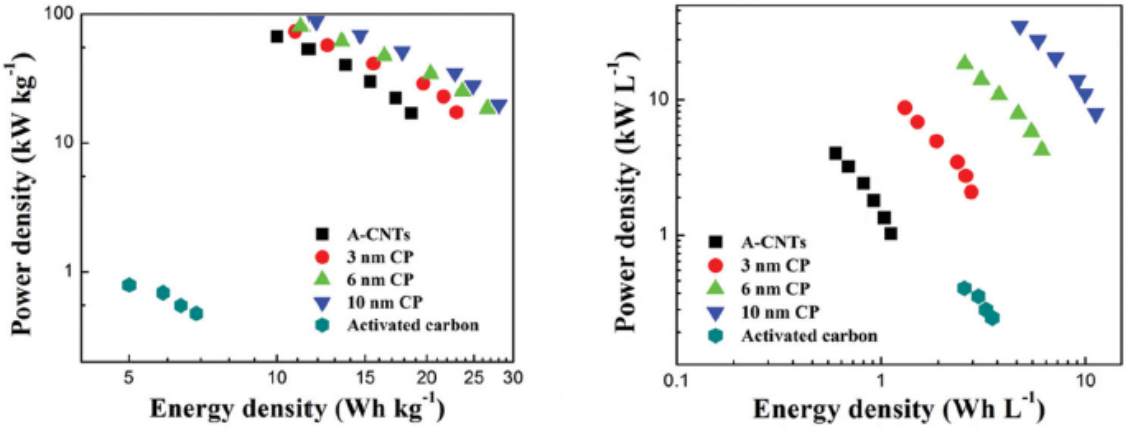

Figure 18. Power vs. energy density trends (Ragone plots) as a function of PEDOT CP thickness over a range of frequencies (0.1 to 0.001 Hz) for cells in 2M BMI-BF 4 /PC. The energy density is proportional to the gravimetric or volumetric capacitance (F/g or F/cm) of the cell and square of the operation voltage (V). Left: Gravimetric densities use the usually assumed dry mass for the electrodes (the positive trend due to PEDOT is thus understated). Right: Volumetric densities use the entire electrode volume (A-CNT, PEDOT and free volume are all included).

1.5 A/aMEGO Electrodes with Wide Operation Temperature

Eutectic Mixtures of Ionic Liquids

Ionic liquids are superior electrolytes that offer larger electrochemical stability range (up to 6 V) compared to organic (2.7 V) and aqueous (1.2 V) electrolytes in addition to their higher thermal and environmental stability One of the limitations of these electrolyte materials is however their low ionic mobility especially below 0ºC temperatures despite their sub-zero melting temperatures. In the last a few years, it was suggested that the formation of eutectic mixtures of ionic liquids is an effective approach to broaden the operation temperature and hence to increase the ionic mobility of these electrolytes at lower temperatures. It was concluded that this increased operation temperature was due to the large stable liquidus temperature range for the mixtures compared to the individual ionic liquids. In other words the size and the symmetry of cations in the eutectic mixture has a substantial effect on the formation of the lattice at lower temperatures and hence on the ionic mobility and melting temperature of the mixture. The crystallization process of the ionic liquids is shown to be mainly influenced by the anions and if the cations are properly selected they can prevent the ordering of the anions and hence shift the gelation and

solidification of the eutectic mixture to the lower temperatures compared to the solidification temperature of the constituents.

Although there have been only a few efforts on the preparation of the eutectic mixtures of ionic liquid for energy storage applications, however, there is no report on the electrolyte system that can operate in the extreme temperature condition (from -50ºC to 80ºC, for instance). Therefore, development of new electrolyte systems that can deliver reliable energy and power in these temperatures is critical and more attention should be diverted to developing these systems. In this section we propose and study a novel eutectic electrolyte system from BMIM BF_4 and 1-butyl-4-methylpyridinium tetrafluoroborate (BMP BF_4) that has the capability of maintaining desirable electrolyte performance at low (down to -50ºC) and high (up to 80ºC) temperatures. Additionally, the new electrolyte has the rate capabilities (up to 100 mV/s) at as low temperatures as -60 ºC. Since the composition of the mixture is 1:1 by weight we will refer to this new electrolyte system as (BMIM $BF_4)_{0.5}$(BMP $BF_4)_{0.5}$. The reason for this selection is that the anions for these two electrolytes are the same and the only difference is on the cations; BMIM ($C_8H_{15}N_2$) is an imidazolium cation and BMP ($C_{10}H_{16}N$) is a pyridinium cation and these two cations have relatively similar structures and side chains with similar values for molecular weights (BMIM BF_4: 226.02 and BMP BF_4: 237.05). It was hypothesized that this slight difference in the cation structure will inhibit the arrangement of the anions and hence will decreases the melting point while enhancing the ionic conductivity. This hypothesis was evaluated using DSC and other measurements that will be discussed in the following sections.

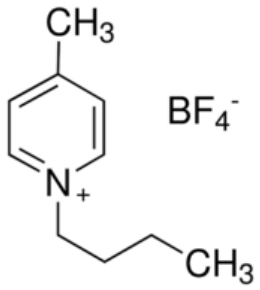

Figure 19. Chemical structure of BMP BF_4.

Preparation of (BMIM $BF_4)_{0.5}$(BMP $BF_4)_{0.5}$ Eutectic Mixture

The eutectic mixture of BMIM BF_4 and BMP BF_4 was prepared by mixing equal amounts of these ionic liquids under an inert nitrogen atmosphere. Prior to the mixing step the two electrolytes were treated at 100ºC for a prolonged period of time (more than 2 weeks) in order to eliminate or minimize the trace amount of impurities. The mixture then was stirred for one day under nitrogen to ensure of uniform blending. Finally the mixture was collected and stored in a vacuum oven under 100ºC for future use. The final eutectic mixture was a clear light brown fluid.

Measuring the Transition Temperatures

DSC measurements were performed in order to analyze the transition temperatures for the pure ILs as well as the mixture. Figure 20 depicts the heating traces of these electrolytes at the temperature range from -90ºC to 30ºC. The melting temperature for BMP BF_4 is observed at -30ºC, while the one for BMIM BF_4 is observed at -39ºC. This difference can perhaps be attributed to the more flat and symmetric structure of BMP cation than that of BMIM cation that results in easier packing and hence higher melting temperature for this electrolyte. There is an additional solid-solid transition for these ionic liquids that take place at

temperatures below their melting points (-58ºC for BMP BF_4 and -77ºC for BMIM BF_4) and can be attributed to recrystallization or glass transition temperatures for these electrolytes. In contrast, the heating trace of the eutectic mixture reveals a shift of the melting temperature to lower temperature of -74ºC. Additionally, it seems that there is no evident solid-solid transition process through slow heating in the mixture at as low temperatures as -90ºC and it indicates that the transition temperature for these processes has also decreased compared to pure ILs. Therefore, by blending BMP BF_4 with BMIM BF_4 the melting temperature for the mixture reduces significantly that is a direct result of dimensional mismatch between the cations in the two electrolytes which impedes the formation of crystallites in the electrolyte mixture.

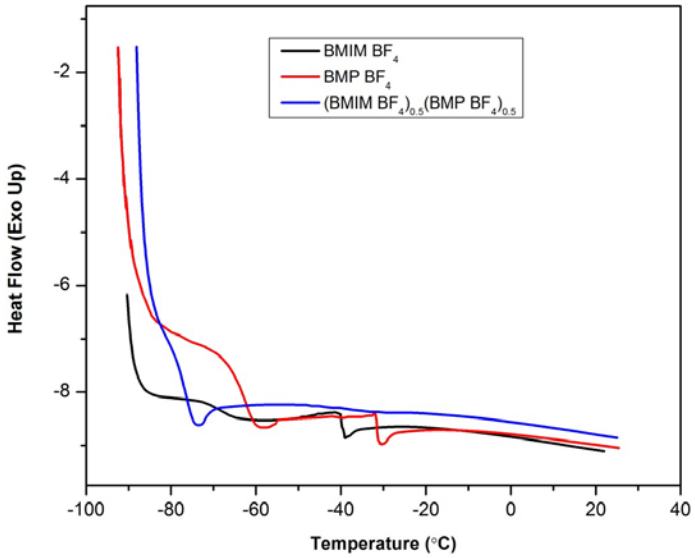

Figure 20. DSC traces of the pure ILs and their eutectic mixture.

Electrochemical Measurements

Cyclic voltammetry and electrochemical impedance spectroscopy measurements were used to investigate the electrochemical behavior of the new electrolyte system. The A-aMEGO-based electrodes were soaked with either pure ILs or the mixture and then the experiments were conducted at the temperature range from -60ºC to 80ºC. At each interval the system was allowed to equilibrate for at least two hours inside the chamber to eliminate the hysteresis from previous experiments. Figures 21 and 22 depicts the normalized CV curves for A-aMEGO-based electrodes with pure BMIM BF_4 and (BMIM $BF_4)_{0.5}$(BMP $BF_4)_{0.5}$ electrolytes respectively as a function of temperature at different scan rates. For the electrodes with pure IL the capacitive behavior is evident at temperatures higher than 20ºC as shown by the nearly rectangular CV curves, although there is some deviation from rectangular shape at 50ºC and 80ºC and this can be related to some impurities or likely chemical reactions in the system at higher temperatures under high voltages. Regardless of the scan rate with pure BMIM BF_4 electrolyte the capacitive behavior almost disappears at temperatures below 0ºC. This can be attributed to the fast diminishing conductivity of this electrolyte at lower temperatures despite its below 0ºC melting temperature. In other words although the pure IL is still liquid at temperatures as low as -50ºC, the high viscosity of the electrolyte (due to gelation before freezing) does not allow the ions to propagate in the

porous electrode system in order to form an EDLC and hence the capacitance reduces significantly. Very similar results were obtained for the electrodes with pure BMP BF_4 as electrolyte with very limited capacitive behavior at temperatures below 0ºC.

On the other hand a very interesting behavior is observed for the eutectic mixture. First, at any temperature electrodes with the eutectic mixture exhibits superior specific capacitance value compared to the ones with pure electrolyte. For instance, at room temperature and 5 mV/s scan rate the specific capacitance with this mixture is 162 F/g while with pure IL the capacitance value is only 136 F/g. This is a direct result of the fact that the mobile ion concentration and hence the ionic conductivity has larger value in the mixture compared to the pure electrolyte. In other words, the addition of BMP BF_4 into BMIM BF_4 reduces the interaction between ionic entities in the pure electrolyte and results in more freedom for the ions to distribute in the porous electrode and reach pores that are not accessible for the ions in the high viscosity electrolytes. Second, electrodes containing the eutectic mixture exhibit capacitive behavior at temperatures as low as -60ºC and again this is due to the improved conductivity of the electrolyte at lower temperatures. For example, the specific capacitance value at -50ºC, 5 mV/s scan rate and 3.5 V peak voltage is calculated to be 92 F/g for the electrodes in the eutectic mixture while under the same condition the capacitance is less than 14 F/g with pure BMIM BF_4. This clearly shows that the eutectic mixture expands the usable temperature range for A-aMEGO-based electrodes between -60ºC and 80ºC with a maximum voltage of 3.5 V.

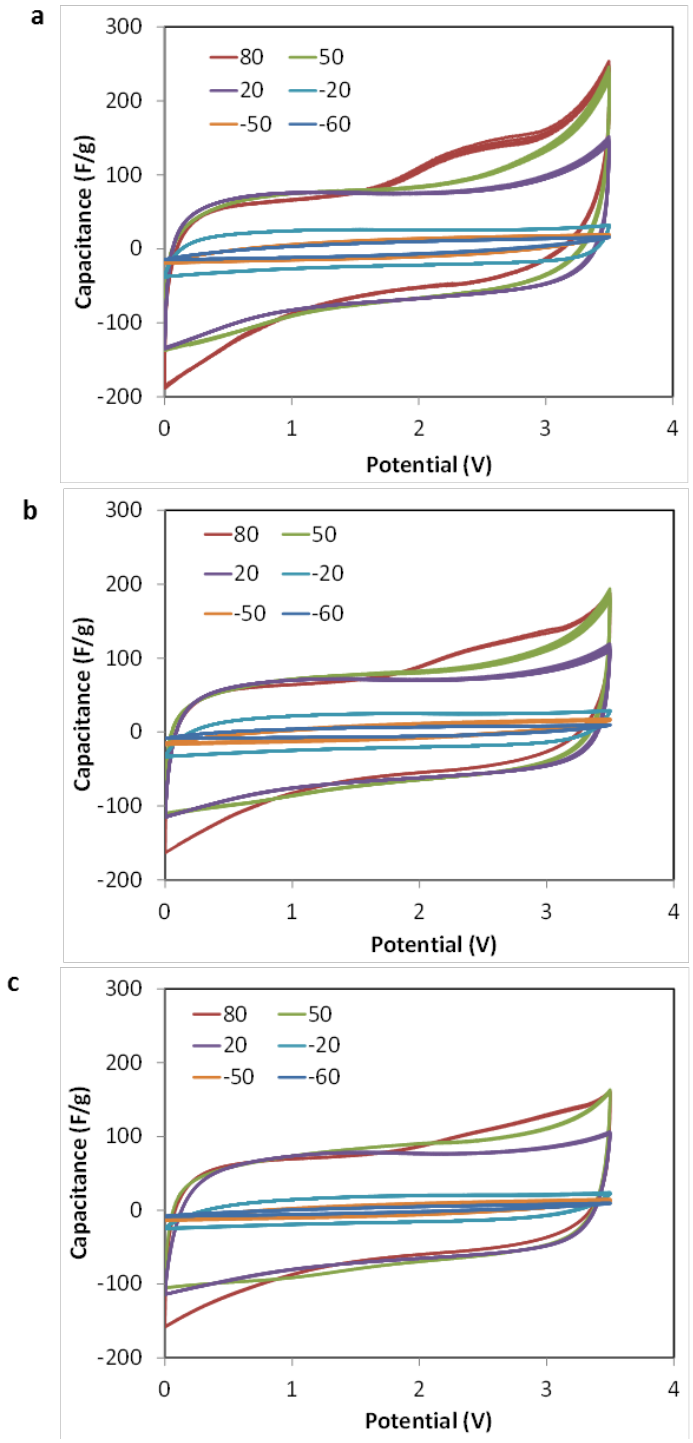

Figure 21. CV curves for A-aMEGO electrodes with pure BMIM BF_4 at different temperatures and scan rates. **(a)** 5, **(b)** 20 and **(c)** 100 mV/s.

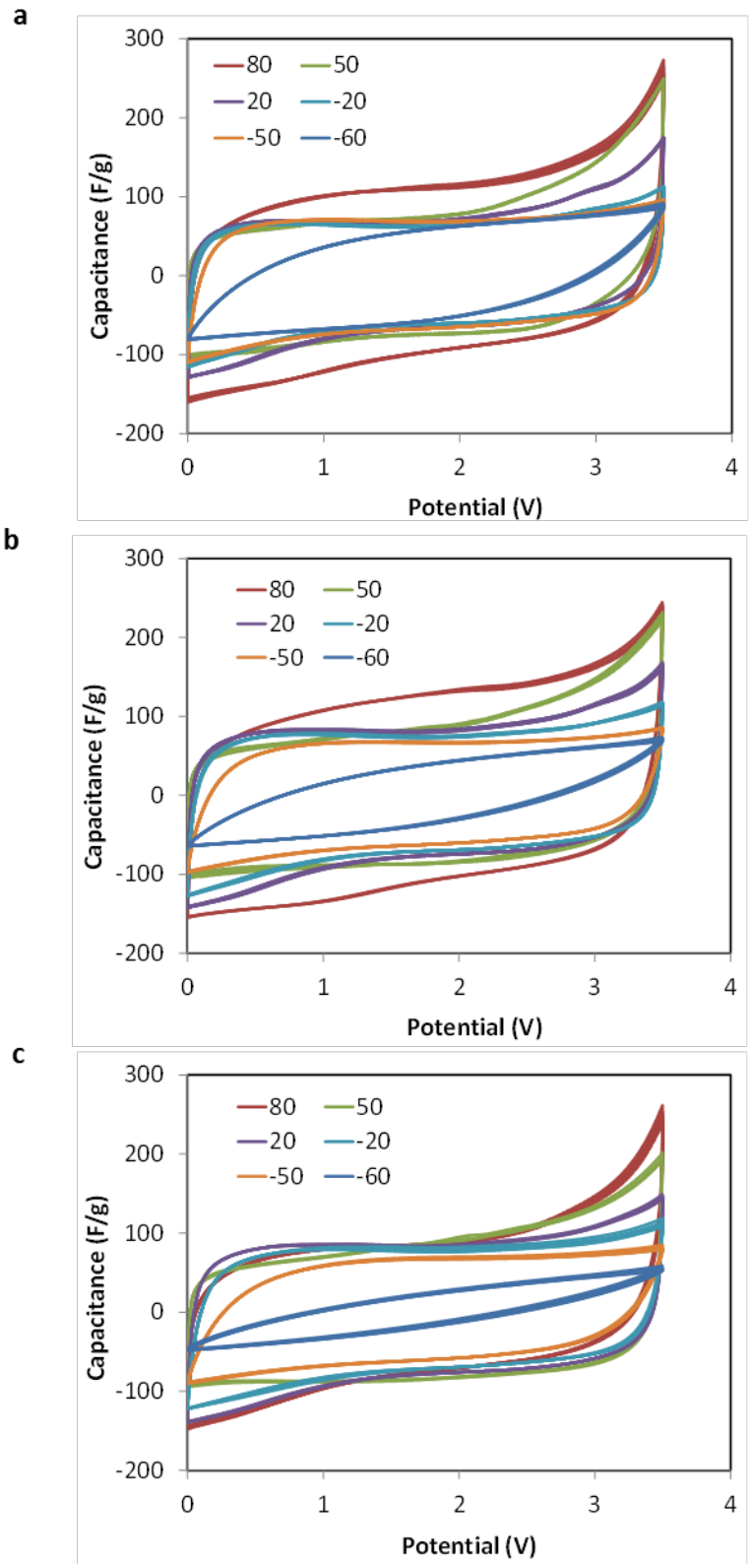

Figure 22. CV curves for A-aMEGO electrodes with $(BMIM\ BF_4)_{0.5}(BMP\ BF_4)_{0.5}$ at different temperatures and scan rates. **(a)** 5, **(b)** 20 and **(c)** 100 mV/s.

Another interesting observation is the rate capability of the electrodes utilizing the newly prepared eutectic mixture, *i. e.* at very low temperatures there is only a minimal drop in the capacitance value by increasing the scan rate up to 100 mV/s. For instance, at -50ºC the specific capacitance value is 83 F/g for 20 mV/s and 77 F/g for 100 mV/s scan rates. The improved ionic conductivity in the eutectic mixture as a result of increased mobile ion concentration renders these free ions to reach micro- and meso-pores in the electrode at very low temperatures that are not accessed by ions in viscous electrolytes. In such viscous electrolytes ions are confined by other ionic entities that limit free mobile ion concentration and therefore the ionic conductivity. Therefore, the eutectic electrolyte system enables A-aMEGO-based electrodes to deliver large amount of power at very low temperatures where batteries or conventional supercapacitors are unable to perform. Only at -60ºC or below the capacitance and power delivery capabilities for the eutectic mixture/A-aMEGO electrode system show noticeable changes.

Further investigation of the electrochemical performance for the newly developed eutectic mixture was conducted by impedance analysis. Figures 23 and 24 depict the Nyquist plots for the electrodes with pure BMIM BF_4 and (BMIM $BF_4)_{0.5}$(BMP $BF_4)_{0.5}$ mixture, respectively. Consistent with the data from CV plots electrodes with pure electrolyte show a relatively small series resistance value at temperatures above 20ºC (7.2 $\Omega.cm^2$ at 20ºC to 2.8 $\Omega.cm^2$ at 80ºC), where the vertical increase in the imaginary part of impedance provides evidence of the capacitive behavior in this temperature range. This is comprehendible since the ionic mobility increases by increasing temperature and results in the reduced series resistance. On the other hand at sub-zero temperatures the size of the semi-circle at high frequency region increases significantly by decreasing temperature as demonstrated by Figure 23b and this can be attributed to the increased series resistance. This is again due to the low conductivity of the pure electrolyte at low temperatures and possible gelation in this system at sub-zero temperatures.

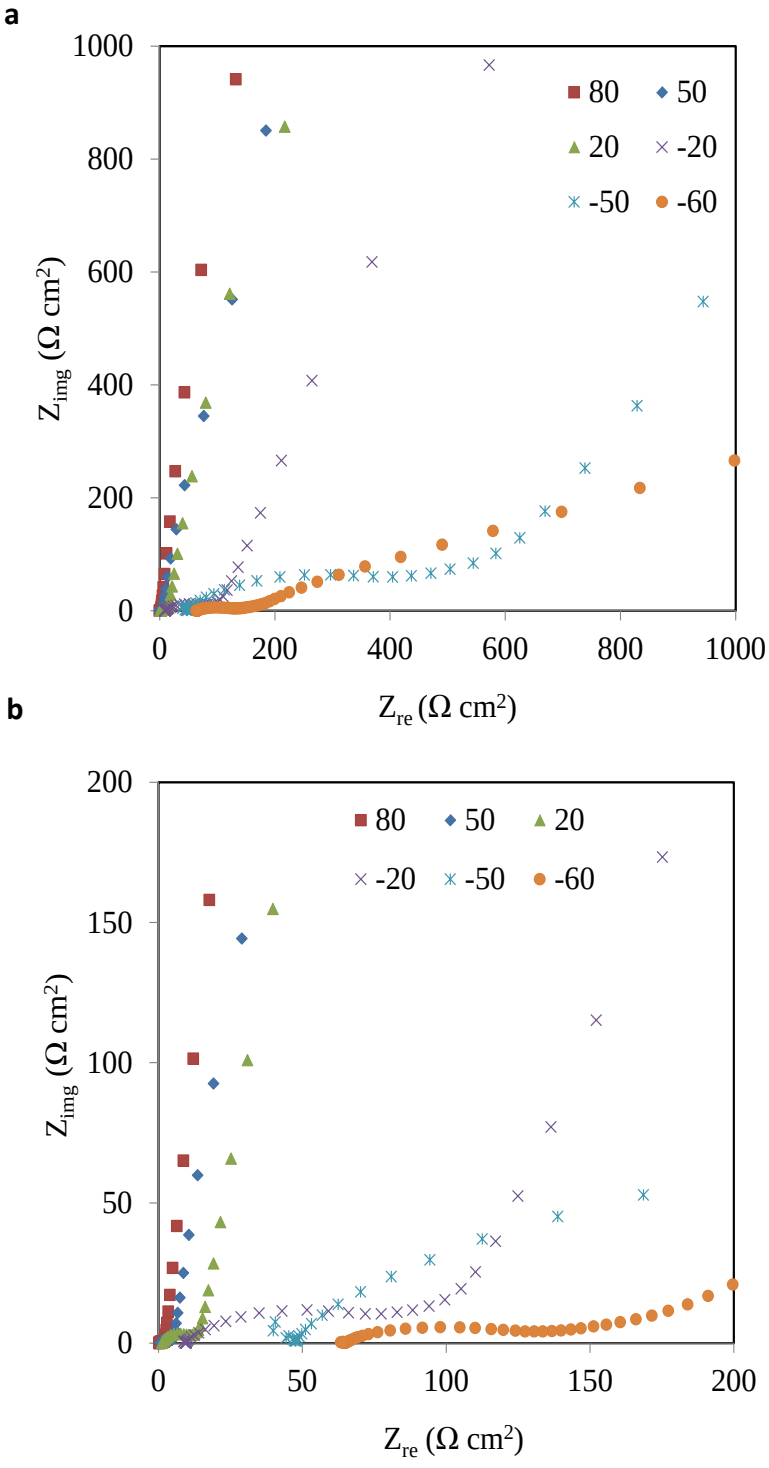

Figure 23. (a) Nyquist plots for A-aMEGO electrodes with pure BMIM BF_4 at different temperatures. **(b)** The high frequency region of the Nyquist plot.

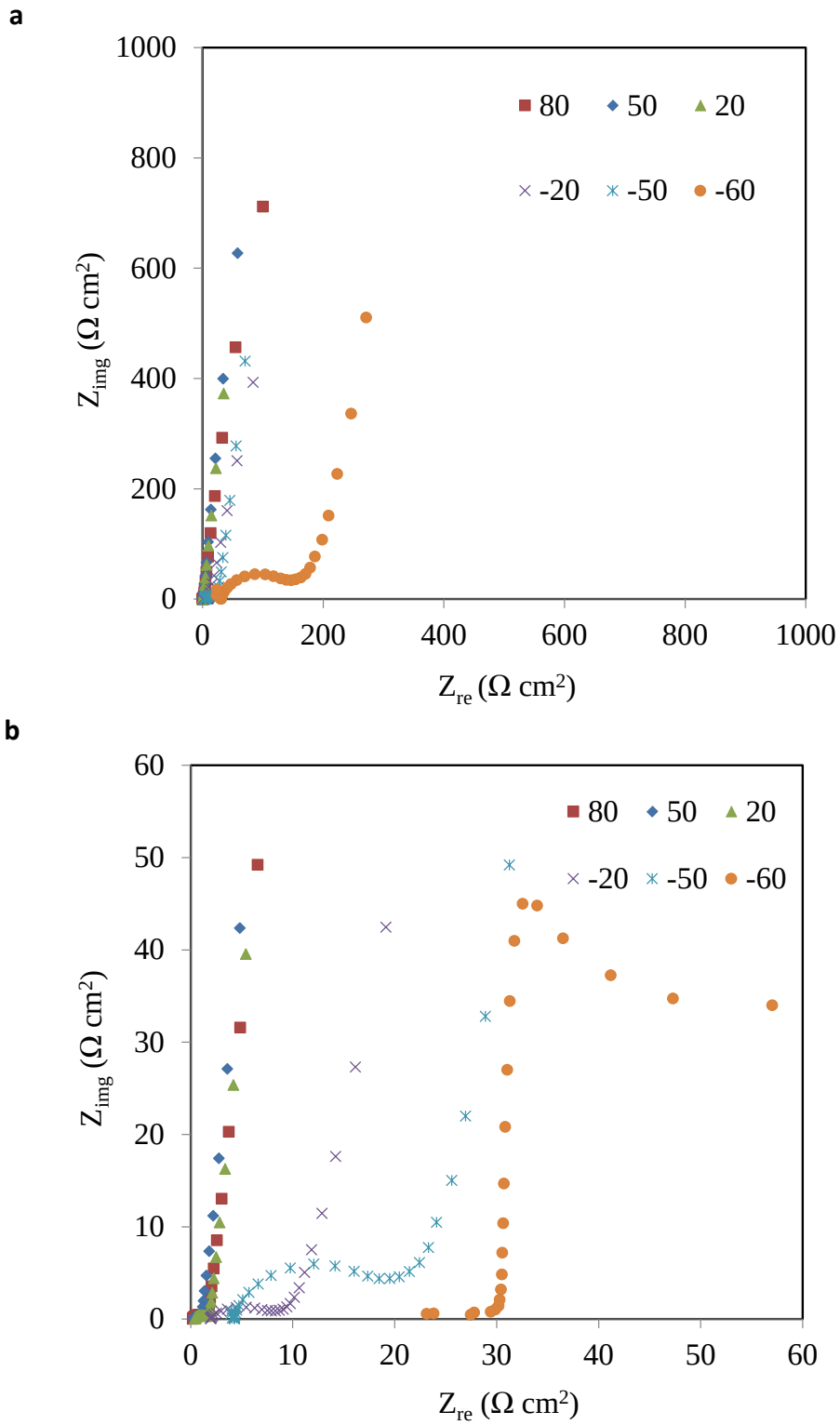

Figure 24. (a) Nyquist plots for A-aMEGO electrodes with $(BMIM\ BF_4)_{0.5}(BMP\ BF_4)_{0.5}$ at different temperatures. **(b)** The high frequency region of the Nyquist plot.

For the eutectic mixture the Nyquist plots of Figures 24a and b show remarkable reduction in the series resistance and the capacitive behavior is observed at all temperature ranges. Although the size of the semi-circle at high frequency region increases by lowering temperature, the very small ESR value of 1.9 $\Omega.cm^2$ was measured at 20ºC and even by lowering the temperature to -50ºC its value still remains as low as 4.7 $\Omega.cm^2$ as shown in Figure 24. Similar to the results from CV plots this reduction in ESR value is linked to the improved ionic conductivity in the eutectic mixture. Similar to result from CV measurements only at very low temperature of -60ºC there is a significant increase in the ESR value and again this can be related to the possible gelation in the electrolyte system at these temperatures. Nevertheless, the electrode with this electrolyte still exhibits capacitive behavior with satisfactory rate capabilities at -60ºC and therefore the eutectic mixture can be used to design and fabricate energy storage systems that can operate in a wide temperature range from -50ºC to 80ºC where conventional batteries or supercapacitors with room temperature ionic liquids (RTILs) are incapable of storing and delivering energy.

2. Asymmetric supercapacitors with high electrochemical performance

2.1 Nanostructured Asymmetric Electrodes for High Performance Energy Storage: Carbon Nanotube/Conducting Polymer Anode and Graphene Cathode

In this work, an asymmetric supercapacitor, exploiting nm-scale conformal coating of a conducting polymer, poly(ethylenedioxythiophene) (PEDOT) on aligned carbon nanotubes (A-CNTs) as the anode, and an ultra-high density activated graphite oxide (a-graphene) as the cathode, has been developed. The asymmetric configuration of the supercapacitor allows both electrodes to be separately tailored, increasing device capacitance and the electrochemical window, and thereby operating voltage. The conformal vapor deposited conducting polymer coating enhances the charge storage of the anode, while the underlying aligned nanowire morphology provides direct non-tortuous fast ion transport pathways to enhance power. The a-graphene cathode, fabricated via a self-assembly process, shows high specific gravimetric and volumetric capacitance for the cathode. As a result of complementary three-dimensional nanotailoring of the asymmetric electrodes, the device exhibits a wide 4V electrochemical window, and the highest power and energy densities reported thus far for carbon-based supercapacitors, 149 kW/L and 113 Wh/L in volumetric performance and 233 kW/kg and 177 Wh/kg in gravimetric performance, respectively.

For supercapacitors, the energy density (*E*) is also related to the gravimetric or volumetric cell capacitance (*C*) and operation voltage (*V*), i.e.,

$$E = \frac{1}{2}CV^2 \tag{6}$$

And the maximum power density P is determined by Equation (4). Equations (4) and (5) indicate that the most effective way to increase the power and energy densities is to raise the cell voltage. In general, the operation voltage of supercapacitors is limited by the electrochemical window (ECW) of the electrolyte which is determined by both the electrolyte and the electrode materials. One promising approach to increase the operation voltage and hence the energy and power densities is to assemble asymmetric supercapacitors that make full use of the electrochemical windows of the anode and cathode combination to increase the maximum cell operation voltage in the devices. Morphology control of the electrodes via

nano-scale tailoring is shown to be an effective way to increase supercapacitor performance (gravimetric and volumetric power and energy) via increasing ECW and capacitance and reducing ESR.

Recent advances in the conformal coating of conducting polymer PEDOT by oxidative chemical vapor deposition (oCVD) onto nanowire arrays and development of graphene with relatively high gravimetric surface area create unique opportunities for developing high performance asymmetric supercapacitors. As schematically illustrated in Figure 25, the combination of the aligned ion transport pathways formed by the aligned nanowire arrays (here, aligned carbon nanotubes, CNTs) that provide fast ion transport in the electrode that reduces ESR of the electrode, and the conformal coating of conducting polymer PEDOT on the A-CNTs that enhances the charge storage capability (a large C) contribute to both high energy and power densities of the cells. PEDOT was selected as the conducting polymer because of its environmental stability, high electrical conductivity, and a wide ECW. As shown in Figure 26(a), conformally-coated oCVD PEDOT on the A-CNTs yields a stable ECW from -1.0 V to 1.8 V, when using an ionic liquid/molecular liquid mixture, 2 M 1-butyl-3-methylimidazolium tetrafluoroborate (BMI BF_4)/propylene carbonate (PC) as the electrolyte. The high ECW of 1.8 V makes it as an excellent anode material in the asymmetric supercapacitors.

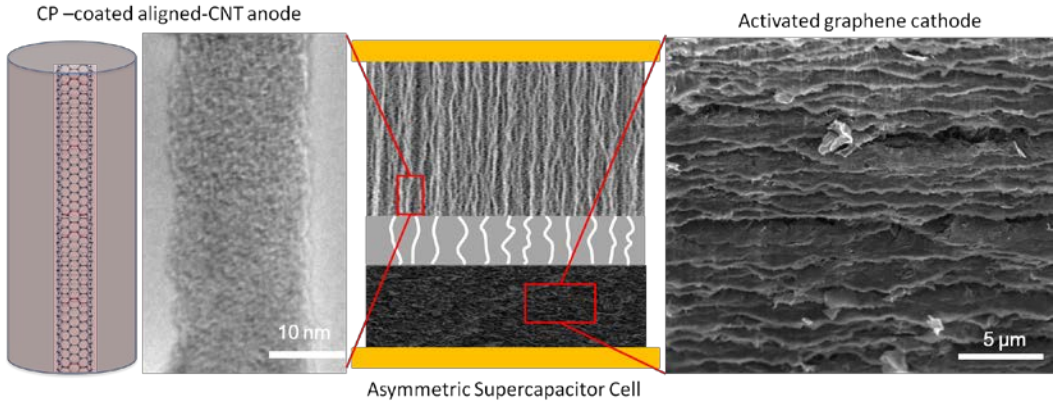

Figure 25. Nanostructured electrodes in asymmetric supercapacitors (left) Low and high magnification TEM micrographs of the anode, comprised of conformal oCVD PEDOT on A-CNTs, and (right) SEM images of activated graphene cathode.

Due to their favorable ECWs, carbon based electrodes such as activated carbon have been used for the cathode in the asymmetric supercapacitors. To significantly improve the capacitance C of the cathode in this study, a new class of carbon material, the activated graphene (a-graphene) was selected due to its superior gravimetric surface area compared with activated carbon. The a-graphene, first reported by Zhu et al, exhibited a very large specific gravimetric surface area (~ 3100 m^2/g) with nano-sized pores and demonstrated a very high gravimetric capacitances of 200 F/g for supercapacitors. However, the simple mechanical packing of the a-graphene flakes caused a low density (~ 0.3 g/cm^3), compared with the graphite density of 2.2 g/cm^3, resulting in a low volumetric efficiency of supercapacitors (the specific volumetric capacitance was 60 F/cm^3). When randomly packing these a-graphene flakes which have lateral dimension of a few microns and a thickness of a few nanometers, it is inevitable to include micron-sized pores in the electrodes, reducing the density. Self-assembly processes are quite effective in increasing the

density of graphene-based materials. Here, by employing a vacuum assisted self-assembly process, which enabled a-graphene flakes aligned in parallel and stacked successively on top of each other, as shown by the SEM image of Figure 25, to fabricate the a-graphene electrodes, the cathode density can be increased markedly to 1.15 g/cm^3 while preserving the nanoporous morphology of each a-graphene flake. To our knowledge, the density of 1.15 g/cm^3 of the a-graphene electrode fabricated here is the highest among the carbon electrodes reported. For example, activated carbon power electrodes fabricated using conventional pressure packing methods have a density of 0.5 g/cm^3. The ECW of the a-graphene was also characterized and as presented in Figure 26(d), the a-graphene has a stable ECW from -2.2 V to 1 V with an electrolyte of 2M $BMIBF_4$/ PC. The combination of high specific gravimetric surface area and high density of the a-graphenes as the negative electrode increases the ECW and results in high volumetric power and energy densities, besides the long cycle lifetime and high capacitive retention.

The asymmetric supercapacitors developed here, consisting of the anode of the conformal coating of oCVD PEDOT on A-CNTs (PEDOT/A-CNTs) and ultra-high density graphene-oxide cathode (HD-a-graphene), can reach a cell operation voltage of 4 V with high capacitance retention after long charge/discharge cycles, demonstrating superior volumetric power and energy densities of 149 kW/L and 113.2 Wh/L, respectively, in addition to high gravimetric electrochemical performance, i.e., a power density of 233 kW kg^{-1} and energy density of 176.6 Wh/kg.

In supercapacitors based on the pure electric double layers (EDL), charge storage is limited to the surface of the porous electrode. In contrast, redox reactions occur throughout the entire volume of conducting polymers (CP), allowing for significantly higher energy storage capability. However, CP electrodes typically suffer poor mechanical stability due to volume changes during the doping/dedoping process, which causes failure of the electrode during long cycling. Recent experiments have demonstrated that the composite approach, in which CP layers are deposited on conductive porous networks such as CNTs, can lead to supercapacitors with significantly improved cycling stability. In such a conductive composite approach, the CNT networks provide electron transport pathways as well as mechanical support to the CP while the deposited CP layers enhance the charge storage capacity of the electrodes.

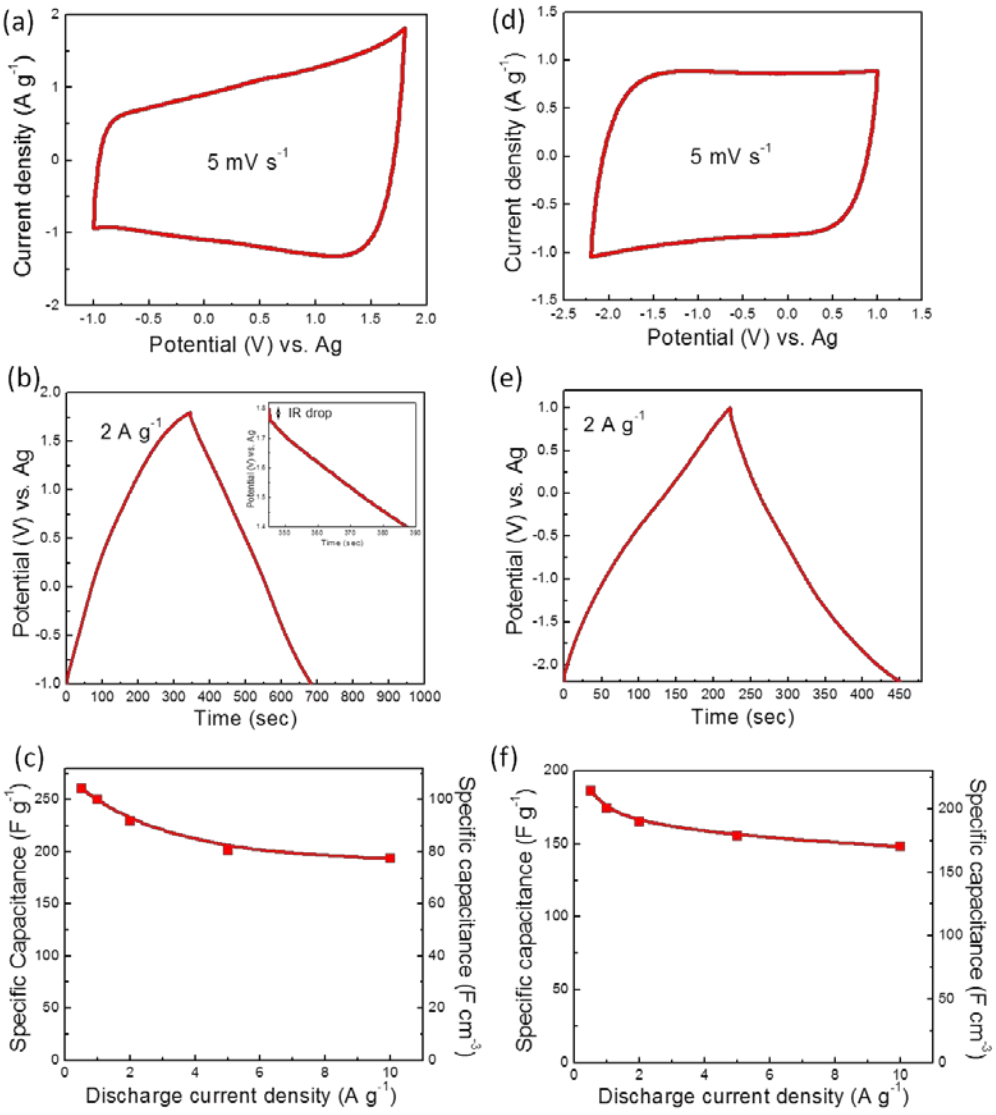

Figure 26. Performance of anode (densified aligned CNTs with conformal CP coating) and cathode (densified graphene) performance (a) CV curves of PEDOT/A-CNTs at 5 mV s^{-1} in 2 M BMIBF4/PC. (b) Galvanostatic charge/discharge curves of PEDOT/A-CNTs composite a current densities of 2 A/g. (c) Specific capacitance at different discharge densities of PEDOT/A-CNTs electrode. (d) CV curves of a-graphene at 5 mV/s in 2 M BMIBF4/PC. (e) Galvanostatic charge/discharge curves of a-graphene at a current densities of 2 A/g. (f) Specific capacitance at different discharge densities of a-graphene electrode.

The high density (via packing) of aligned carbon nanotube (A-CNT) forests are distinctively advantageous as the conductive networks to support the CP coating layer in supercapacitors, relative to randomly packed morphologies. Apart from the direct (and thereby fast) ion transport to reduce ESR, as illustrated in Figure 25, the PEDOT/A-CNTs also provide better mechanical stability and hence higher retention of the capacitance after long charge/discharge cycles, compared with the electrodes of the

PEDOT/randomly packed CNT networks. In the extant literature, electrodes of CP/CNTs were fabricated by electrochemical methods, which will result in non-uniform CP layers on the CNTs. In Figure 25, the thin (~5 to 10 nm) oxidative chemical vapor deposition (oCVD), PEDOT layers forms a conformal coating on very high aspect ratio A-CNTs (0.2 mm long). The A-CNTs in this study were grown by a modified thermal CVD method at atmospheric pressure. These as-grown CNTs have a highly aligned structure with approximately 1% volume fraction (Vf) corresponding to ~80 nm inter-CNT spacing and an average CNT diameter of 8 nm. In order to achieve high volumetric performance of the device, the PEDOT/A-CNT forests were mechanically densified to 5% Vf of A-CNTs.

The electrochemical performance of PEDOT/A-CNTs anodes were evaluated by cyclic voltammetry (CV) and galvanostatic charge-discharge tests using a screen-printed electrode system (Dropsens) with the PEDOT/A-CNTs and a Pt current collector as the working electrode, while Ag and Pt were used as the reference and counter electrodes, respectively. Figure 26(a) presents a CV curve of the PEDOT/A-CNTs electrode in 2 M $BMIBF_4$/PC at a scan rate of 5 mV s^{-1}, which shows an ECW of -1 V to +1.8 V. The galvanostatic cycles for the PEDOT/A-CNTs electrode at 2A g^{-1} are presented in Figure 26(b). The symmetric and linear charge and discharge characteristics reveal a rapid I-V response and reversible electrochemical reaction, resulting in an excellent capacitive behavior. The capacitance of the electrode was determined from Equation (1). A high specific gravimetric capacitance of 230 F/g was obtained at 2 A/g. Figure 26(c) presents the specific capacitance at different discharge current density, from 0.5 A/g to 10 A/g. Capacitance retention of 74.2% was obtained at 10 A/g (from 260.8 F/g at 0.5 A/g to 193.5 F/g at 10 A/g), indicating that the PEDOT/A-CNTs electrode provide reliable capacitive performance for high power applications.[8] This relatively high retention mechanistically arises from the conformal coating of oCVD PEDOT on A-CNTs. The parallel ion transport pathways formed by the PEDOT/A-CNTs, and the high electronic conductivity of the A-CNTs, improve the ion transport and result in low ESR and therefore high power density. The cycling stability of the PEDOT/A-CNTs electrodes was characterized and compared with that of the electrodes of PEDOT deposited on randomly packed CNT networks. Symmetric supercapacitors made of the PEDOT/A-CNTs had a retention of 89% after 1000 cycles of 2 V voltage cycle, compared with a retention of 73% after 1000 cycles from PEDOT on random CNT morphologies. At lower voltage of 1 V, the retention of the PEDOT/A-CNTs was increased to 94% while that of the PEDOT on random CNT networks was at 88%. In the randomly packed CNT networks, there are CP layers in the gaps between CNTs and after long charge/discharge cycles, the mechanical failure of CP layers in these gaps will cause disruption of the electric conduction paths between CNTs and reduce the conductivity of CNT networks. As a result, the capacitance is reduced. In contrast, the electric conduction path of the continuous aligned CNTs would not be disrupted by the mechanical failure of the CP coating layers due to the A-CNT/CP morphology. Hence, the A-PEDOT/A-CNTs electrodes exhibit more robust mechanical stability and high retention of the capacitance, compared with the electrodes of the CP deposited on randomly packed CNT networks.

The electrochemical performance of the a-graphene electrode was characterized as above including using. 2 M $BMIBF_4$/PC as the electrolyte. Figure 26(d) presents a CV curve of the a-graphene electrode at a scan rate of 5 mV/s showing an ECW of -2.2 V to +1 V. The slope of the discharge curve in Figure 26(e) (Equation (1)) yields a specific capacitance of 165 F/g at 2 A/g. The specific capacitances of the a-graphene electrode with different discharge currents are presented in Figure 26(f). The a-graphene electrode exhibits high specific capacitance, ranging from 186.4 F/g to 148.2 F/g as the discharge current increases from 0.5 A/g to 10 A/g. It should also be mentioned that the specific capacitance of 175 F/g at 1

A/g discharge current is the same as that measured by Zhu et al. on a-graphene electrodes fabricated using the traditional mechanical packing method which yields specific capacitance > 150 F/g obtained from the discharge curve with a constant current of 0.8 A/g. Moreover, the high density of the a-graphene electrodes results here in a specific volumetric capacitance with 175 F/cm^3 from the discharge curve of constant current of 1 A /g, which is the highest among all the carbon based electrodes.

Both electrodes are independently tailored in asymmetric supercapacitors to operate under more optimal conditions. Here, the PEDOT/A-CNTs anode and a-graphene cathode were assembled, separated by a porous paper of 40 μm thick. 2 M BMIBF4/PC was used as the electrolyte due to its high ionic conductivity. By properly tuning the mass ratio of the two electrodes, the asymmetric capacitor can be operated at the full 4 V cell operation voltage, reaching the maximum voltages from both electrodes (= 1.8 V (anode, A-CNTS PEDOT, V_+) + 2.2 V (cathode, a-graphene, V_-)). From the consideration that charge stored at the two capacitor electrodes should be equal in magnitude with opposite sign ($|q_+| = |q_-|$), and the stored charge q at the electrode is, $q = C\,\Delta V\,m$, where C is the specific gravimetric capacitance, ΔV is the maximum potential range allowed by the ECW, and m is the mass of the electrode, the mass ratio between the two electrodes can be determined,

$$\frac{m_+}{m_-} = \frac{C_-\Delta V_-}{C_+\Delta V_+} \tag{7}$$

From the specific capacitances of the positive and negative electrodes, 230 F/g and 165 F/g, respectively, at a constant discharge current of 2 A/g, and ΔV_+ =1.8 V and ΔV_- = -2.2 V, Equation (7) yields the mass ratio (m_+/m_-) of 0.88, for a full 4 volts cell operation voltage, providing the design characteristics of the asymmetric supercapacitor assembled here.

Figure 27(a) presents the CV curves of the fabricated asymmetric supercapacitors at scan rates from 5 to 100 mV s^{-1} using the 2 M $BMIBF_4$/PC as electrolyte. The capacitors display near rectangular CV curves, especially for the lower scan rates. In order to evaluate the capacitive performance of the cell further, galvanostatic charge/discharge curves at different current densities were characterized. The galvanostatic cycles at alternate charge/discharge current densities of 2 A/g and –2 A/g were presented in Figure 27(b), from which the cell capacitance was determined (Equation (1)). Figure 27(c) presents the cell gravimetric and volumetric capacitances at different discharge currents. It should be noted that the calculated cell capacitance was based on the total mass of the active materials (both positive and negative electrodes) because it is not meaningful to deduce the specific capacitance of a single electrode for the asymmetric supercapacitor. The cell capacitance is 81.6 F/g at 0.2 A/g and becomes 55.4 F/g as the discharge current density increases to 10 A/g, indicating relatively good capacitance retention. The cell capacitance obtained here is higher than that of a-graphene based symmetric supercapacitors and other conducting polymer based asymmetric supercapacitors. Cycling stability of the asymmetric supercapacitors was demonstrated by continuously cycling the galvanostatic charge/discharge process between 0 and 4 V at a current density of 5 A/g for more than 1,000 cycles. As shown in Figure 27 (d), the asymmetric supercapacitor maintains electrochemical retention of 94% after 1,000 cycles. The small capacitance loss is likely attributable to capacitance decay of the PEDOT/A-CNTs anode.

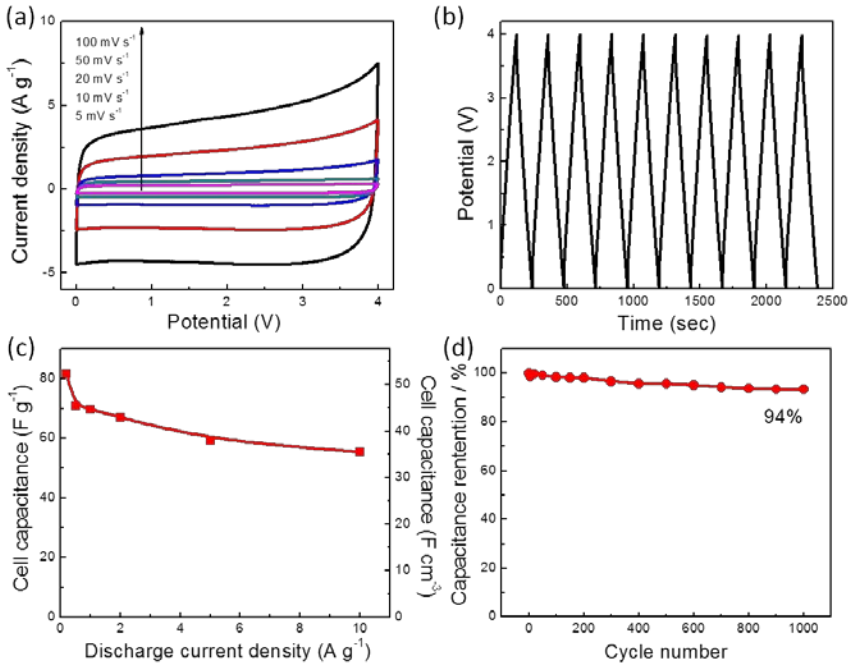

Figure 27. Asymmetric supercapacitor performance (a) CV curves of PEDOT/A-CNTs//a-graphene asymmetric supercapacitor at different scan rates of 5, 10, 20, 50 and 100 mV/s between 0 and 4 V in 2 M BMIBF4/PC electrolyte. (b) Galvanostatic charge/discharge curves of asymmetric device at a current density of 2 A/g. (c) Cell capacitances of asymmetric cell at different discharge current densities. (d) Cycle capacitance retention of asymmetric supercapacitor under a voltage of 4 V at a current density of 5 A/g in 2 M BMIBF4/PC electrolyte.

The electrochemical performance of the asymmetric supercapacitor cell was further characterized by electrochemical impedance spectroscopy (EIS). Presented in Figure 28(a) is the Nyquist plot obtained in the frequency range of 100 kHz to 10 mHz of 5 mV applied voltage, which shows a semicircle in the high frequency region and a sharp rise of the imaginary part of the electric impedance, reflecting the dominance of the cell capacitance in the low frequency region. The semicircle in the Nyquist is attributed to the charge transfer resistance of the porous electrodes. The high frequency intersection of the semicircle on the real axis of the Nyquist plot represents the internal resistances including Ohmic resistance of the electrolyte, the resistance of the electrode materials, and resistance in the separator, and the contact resistances between active materials and current collector. The cell shows an internal resistance with 0.1 Ω cm^2 when normalized with the area of the current collector of the capacitors indicating a high electrical conductivity and low ESR of the cells.

The maximum power density of the asymmetric capacitors was determined from Equation (4). The ESR in Equation (3) can be deduced from the data in Figure 26(b) with Equation (3). Figure 28(c) presents the Ragone plot (gravimetric power density versus energy density) of the asymmetric supercapacitor derived from the galvanostatic discharge curves measured at different charge/discharge current densities. In addition to gravimetric performance, the maximum power density is derived from Equation (4) where *V* is the operation voltage, which is 4 V here.

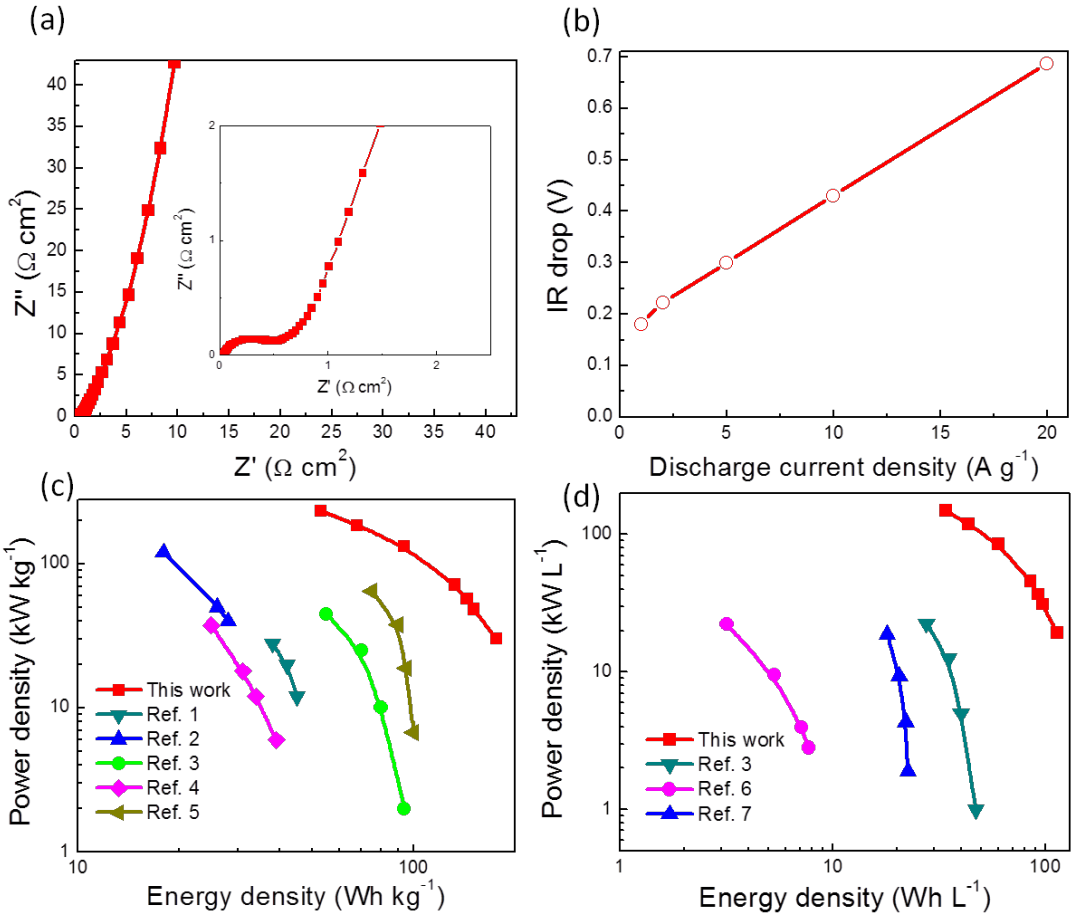

Figure 28. Asymmetric cell absolute and relative performance (a) Nyquist plot of the asymmetric cell. (b) IR drop with different current densities. (c) Ragone plot of PEDOT/A-CNTs//a-graphene asymmetric supercapacitor in gravimetric unit. (d) Ragone plot of PEDOT/A-CNTs//a-graphene asymmetric supercapacitor in volumetric unit.

References: 1. Choi, B. G. et al., *ACS Nano* **6**, 4020-4028 (2012). 2. Chen, P. C. et al., *ACS Nano* **4**, 4403-4411 (2010).3. Izadi-Najafabadi. et al., *Adv. Mater.* **22**, E235-E241 (2010).4. Wang, Z.-L. et al., *Scientific reports* **3** (2013). 5. Zhi, M. et al., *J. Power. Sources.* **208**, 345-353 (2012). 6. Raymundo-Piñero. et al., *ChemSusChem* **4**, 943-949 (2011). 7. Chen, Z. *et al.*, *Advanced Energy Materials* **1**, 551-556 (2011).

The volumetric energy and power densities are more important in practical applications. Figure 28(d) presents a comparative Ragone plot of asymmetric cells in terms of the volumetric performance. The cells exhibit both high volumetric and gravimetric power and energy density at 149 kW/L (233 kW/kg) and 113.2 Wh/L (176.6 Wh/kg), respectively. These values are significantly higher than those of other reported carbon based symmetric supercapacitors, conducting polymer based supercapacitors and other devices reported previously as compared in Figures 28(c) and 28(d). The pseudocapacitor nature of PEDOT has lower charge/discharge speed compared with that of the pure EDLC supercapacitors and hence the power

density is lower than that of the A-aMEGO supercapacitors, which have been presented in the proceeding section.

An asymmetric supercapacitor, exploiting the conformal coating of PEDOT on A-CNTs as the anode which combines fast ion transport pathways, enhances charge storage capability, and reduces ESR, and the a-graphene cathode fabricated from a self-assembly process which possesses exceedingly high specific gravimetric and volumetric capacitance, has been developed in this paper. The anode and cathode materials are individually tailored to control spacing and alignment of graphene and CNTs, and work synergistically together in the asymmetric cell configuration by expanding the ECW. The unique nanomorphology of the conformal coating of CP on A-CNTs also imparts mechanical stability and high cycle retention of the capacitors, compared with electrodes comprised of CP deposited on randomly packed CNT networks. Tailoring of the anode and cathode materials at a scale approaching that of the ions can allow asymmetric supercapacitor performance to be further expanded, e.g., utilizing other conducting polymers besides the PEDOT demonstrated here, as well as other high performance carbon based cathodes such as high volume density A-CNTs to meet the requirement of a broad range of energy storage applications.

3. Asymmetric Supercapacitor Based on Conducting Polymer and Aligned Carbon Nanotubes with Controlled Nanomorphology

In this program, an asymmetric supercapacitor, exploiting the earlier mentioned nm-scale conformal coating of conducting polymer (CP) on A-CNTs as the negative electrode and an ultra-high density A-CNTs as the positive electrode, has been developed. The conformal CP coating on the A-CNTs enhances charge storage while the aligned nanotube morphology provides straight and fast ion transport pathways. The A-CNTs electrode, densified by a unique mechanical method, possessing high volumetric capacitance while preserving the aligned morphology to maintain the high power, provides an ideal positive electrode for the asymmetric supercapacitor. By complementary tailoring of the asymmetric electrodes, the device exhibits a wide operation voltage of 4 V with the high energy and maximum power densities as 82.8 Wh L^{-1} and 130.6 kW L^{-1} in volumetric performance. In this work, a new method was introduced which is simple but can determine directly the energy storage efficiency of a supercapacitor cell. An equivalent circuit was developed to model the performance of each electrode and investigate the asymmetric design of the cell.

The energy density (E) of supercapacitor depends on the gravimetric or volumetric cell capacitance (C) and operation potential (V) with Equation (5). And the maximum power density Pmax is determined by Equation (4). The cell capacitance is determined mainly by the electrode materials and the operation potential is related to the electrochemical window (EW) of the electrolyte and electrodes. Equations (1) and (2) indicate that one of effective ways to increase the maximum power and energy densities is to raise the cell voltage. One promising approach to increase the operation voltage and hence the energy and maximum power densities is to assemble asymmetric supercapacitors which combine the battery-like pseudocapacitve electrode, such as the redox active materials of transition metal oxides or conducting polymers (CPs) which have high energy density, and the electric double layer capacitor (EDLC) electrode which provides high power density. The asymmetric configuration will take the advantage of different electrochemical windows in both electrodes to increase the cell operation voltage, resulting in an improved specific capacitance, energy and power densities.

As in previous work, composite electrodes combining PEDOT and A-CNTs were fabricated. As shown in Figure 29(a), the A-CNTs provide the parallel pathways to enhance the ion transport speed, reduce the electric resistance and improve the ion accessibility under the higher current density. In order to achieve both high gravimetric and volumetric performance of the cell, the ultrahigh density A-CNTs electrode was densified via a mechanical compression process to 40% volume fraction (Vf) shown in Figure 29(b). For the other electrode, a modified chemical vapor deposition (o-CVD) was employed to deposit PEDOT (which has higher conductivity and wider potential window compared with other conducting polymer) on the A-CNTs. As shown in Figures 29(c) and 29(d), nanometer thin PEDOT layer is deposited as the conformal coating on the A-CNTs, preserving the nanomorphology of aligned ion transport pathways of the A-CNTs. The composite electrodes thus fabricated possess high mechanical stability and hence a long cycling life compared with that of CP deposited on randomly packed CNTs. The PEDOT/A-CNTs electrode was also densified via the mechanical compression process to 5% Vf. Based on the EW as shown in Figure 30(a), the PEDOT/A-CNTs was used as the negative electrode (see illustration in Figure 29(d)). The ultrahigh density A-CNTs are utilized as the positive electrode, and this combination provides the asymmetric supercapacitor with 4 V operation voltage, much higher than each individually electrode.

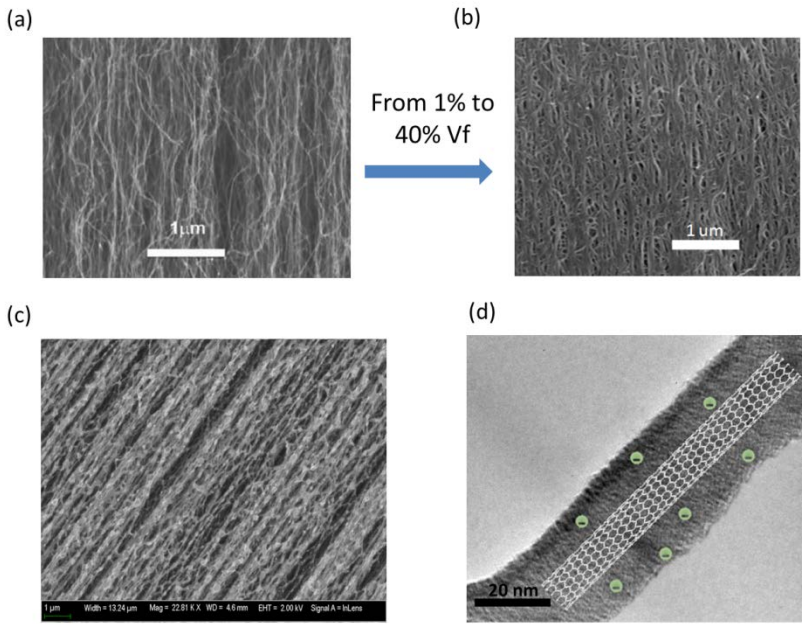

Figure 29. Microstructure of supercapacitor electrodes. SEM images of (a) as grown A-CNTs with 1% Vf and (b) densified A-CNTs with 40% Vf. (c) SEM images of PEDOT/A-CNTs composite. (d) Scheme and high magnification TEM images of a single PEDOT coated A-CNT electrode. A CNT is drawn to illustrate the conformal coating of PEDOT on A-CNTs. Negative ions are drawn to illustrate the ion storage in the entire volume of the PEPOT electrode.

It should be noted that the coulombic efficiency is another important parameter for supercapacitors besides the energy and power densities. The coulombic efficiency measures the electric energy losses of supercapacitors in charge/discharge cycles. A high performance supercapacitor (near ideal capacitor) should have the efficiency as high as 90%. In the asymmetric supercapacitors reported here, the A-CNTs provide the aligned ions transport pathways to reduce the ESR, and hence reduce the energy loss.

Meanwhile, we introduce a simple and more direct method, i.e., Charge-Voltage (Q-V) curves, which can provide accurate measure of the efficiency compared with traditional method reported in the literature.

To better understand the working mechanism of the asymmetric pseudocapacitances, an equivalent circuit was developed based on the electrochemical impedance spectroscopies (EIS) of individual electrodes and the asymmetric supercapacitor cell over a broad frequency range. It is noted that in the extant literature, there is few work concerning about the fitting for both pseudocapacitive and EDLC type electrodes, as well as the asymmetric cell. The asymmetric electrochemical cell here provides an opportunity to study these two types of electrodes because both electrode materials are A-CNTs based. The complicated charge/discharge process will be represented as different circuit elements to investigate the equivalent capacitance, ion diffusion coefficient and other parameters. The modeling of the asymmetric cell will also provide vital information for the data from three-electrode and two-electrode measurements and studying whether each electrode is optimized for the asymmetric cell.

To investigate the electrochemical property of as-synthesized PEDOT/A-CNTs and ultrahigh density A-CNTs electrodes, CV measurements were carried out on the two electrodes using screen-printed three electrodes system (Dropsens), where silver and platinum were used as reference and counter electrodes, respectively. 2 M $BMIBF_4$/PC was used as electrolyte because of wide electrochemical window and high conductivity. As shown in Figure 30(a), a potential window of -2.2 V to 1.3 V was obtained at a scan rate of 100 mV s^{-1} for the A-CNTs electrode. In contrast, the PEDOT/A-CNTs composite electrode shows an electrochemical window from -1 V to 1.8 V at the same scan rate. The quasi-rectangular CV curve for the PEDOT/A-CNTs composite electrode reveals that the electrode preserves the nanomorphology of aligned ion transport pathways (due to the A-CNTs) that enable fast ion transport in and out of the electrode and a reversible doping/dedoping process of the PEDOT coating layer. The doping process of PEDOT is presented as

$$CP \rightarrow CP^{n+} + ne^{-} \quad (8)$$

In the cathode, the negative ions will screen the positive charges of CPn+ as CPn+ + (A-)n, where CP is the conducting polymer, A^{-} is the negative ion of the electrolyte, in the bulk of the conducting polymer. Compared with EDLCs based on carbon in which ions' sorption and desorption determine cell performance, supercapacitor based on conducting polymer stores charges in the bulk of the active materials, i.e., the conducting polymer. The specific capacitance can be calculated through integrating the discharge part of CV curve. The data show that the volumetric specific capacitance of PEDOT/A-CNTs is larger than that of A-CNTs, because of the higher volumetric capacitance of the pseudocapacitance of the composite electrode, as expected.

The galvanostatic cycle measurements were performed to quantify the specific capacitance and investigate the electrochemical behavior of the electrodes. The charge/discharge curve for the PEDOT/A-CNTs electrode at alternate current density of 1 A g^{-1} and -1 A g^{-1} based on the three electrode system in 2 M BMIBF4/PC is presented in Figure 30(b). From the slope of the galvanostatic curves, dV/dt, the capacitance of the electrode can be determined by Equation (1). From the data in Figure 30(b), a specific capacitance of 205 F g^{-1} for PEDOT/A-CNTs electrode is deduced for the current density of 1 A g^{-1}. A specific capacitance of 121 F g^{-1} is obtained for the densified A-CNTs electrode at 1 A g^{-1} from the discharge curve. Figure 30(c) presents the volumetric specific capacitances of both electrodes versus discharge current density, from 0.5 A g^{-1} to 10 A g^{-1}. The data show that the PEDOT/A-CNTs

pseudocapacitor electrodes have a high capacitance retention of 71% (from 110.5 F cm^{-3}/245.6 F g^{-1} at 0.5 A g^{-1} to 78.4 F cm^{-3}/174.3 F g^{-1} at 10 A g^{-1}). This high capacitance retention arises from the uniformly coating of PEDOT on A-CNTs, as shown in Figure 29(d), which preserve the nanomorphology of parallel ion transport pathways formed from the PEDOT/A-CNTs and high electronic conductivity of the CNTs which improve the ions transport and result in high power density.

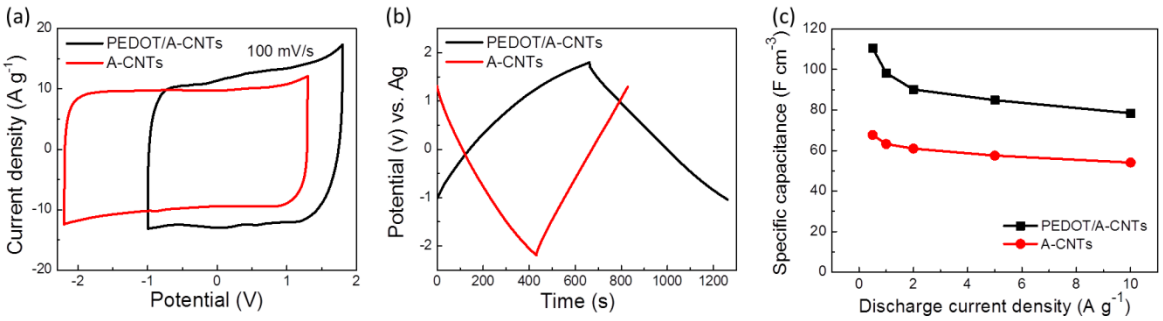

Figure 30. Electrochemical performance of each electrode. (a) CV curves of both electrodes at 100 mV s^{-1} in 2 M $BMIBF_4$/PC. (b) Galvanostatic charge/discharge curves of both electrodes at 1 A g^{-1} 2 M $BMIBF_4$/PC. (c) Specific volumetric capacitances at different discharge densities of both electrodes.

The results in Figure 30(a) show the stable potential windows of -2.2 V to 1.3 V for the ultrahigh density A-CNTs electrode and of -1 V to 1.8 V to the PEDOT/A-CNTs electrode obtained in the 2 M BMIBF4/PC using Ag as the reference electrode. Thus, the operation window of asymmetric supercapacitor can be extended up to 4 V (2.2 V for ultrahigh density A-CNTs plus 1.8 V for PEDOT/A-CNTs) by tuning the mass (volume) ratio of the two electrodes. Since the charges stored in the two capacitor electrodes should be equal in magnitude with opposite signs ($|q_+| = |q_-|$), the mass ratio between the two electrodes can be determined from the electrochemical windows of the two electrodes. For a capacitor electrode, the stored charge q is:

$$q = C\Delta Vm \qquad (9)$$

where C is the specific gravimetric capacitance, ΔV is the maximum potential range allowed by the electrochemical window, and m is the mass of the electrode. From ($|q_+| = |q_-|$), the mass ratio between the two electrodes is determined by Equation (6). For the asymmetric capacitor developed here, the specific capacitances of the PEDOT/A-CNTs and ultrahigh density A-CNTs electrodes are 205 F/g and 121 F/g, respectively, at a constant discharge current of 1 A/g. The optimal mass ratio of the two electrodes can be deduced to be 0.72. Thus, the asymmetric supercapacitors were assembled with the mass ratio of 0.72 between the PEDOT/A-CNTs and ultrahigh density A-CNTs electrodes, separated by a 25 mm thick porous membrane (Celgard 3501, Celgrad LLC) while 2 M $BMIBF_4$/PC was used as the electrolyte.

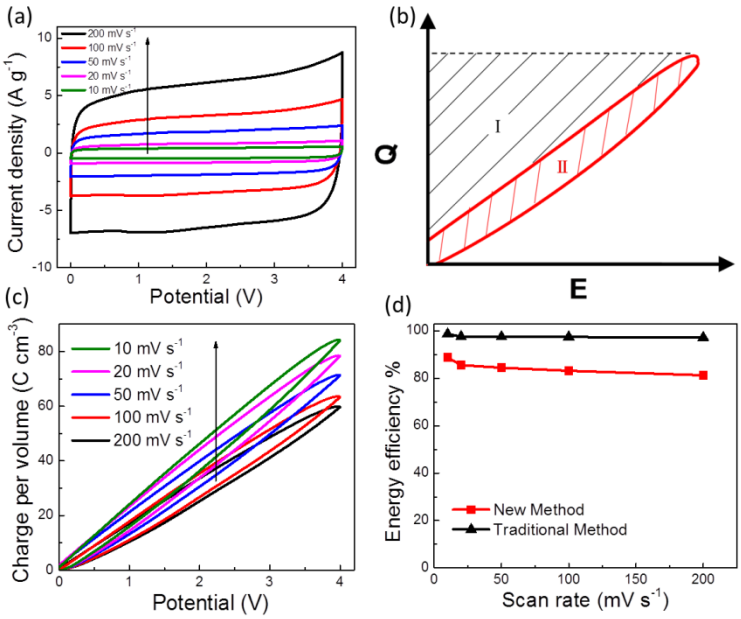

Figure 31. Electrochemical performance of asymmetric PEDOT/A-CNTs// ultrahigh density A-CNTs cell. (a) CV curves of asymmetric cell at different scan rates of 10, 20, 50, 100 and 200 mV s^{-1} between 0 and 4 V in 2 M $BMIBF_4$/PC electrolyte. (b) Typical QV curve of supercapacitor cell. (c) QV curve of cell at different scan rates between 0 and 4 V. (d) coulombic efficiency of asymmetric cell with different scan rates.

Figure 31(a) presents the CV curves of the asymmetric capacitor thus fabricated at different scan rates of 10, 20, 50, 100, 200 mV s^{-1} between 0 and 4 V for a two-electrode measurement system. The cell shows a near rectangular shape CV curve especially under small scan rate, indicating an ideal capacitive behavior under 4 volts operation. Besides the energy and power densities, the energy storage efficiency, which is directly related to the loss of a supercapacitor in the charge/discharge process, can be used to describe how ideal the capacitive behavior of the cell is. We note that the coulombic efficiency which is the ratio of total charges between discharging and charging process deduced from the CV curves in Figure 31(a) was used to describe the performance of a supercapacitor. Here, we show that although the coulombic efficiency can provide an approximate estimation of the energy storage efficiency (and hence the loss), one can evaluate from the CV curves in Figure 31(a) exactly the energy storage efficiency and loss of a supercapacitor during a charge/discharge cycle using a QV curve as shown in Figures 31(b) and 31(c). From the total power *V*I, where *V* is voltage and I is current, delivered to or from a supercapacitor, the total input electric energy to a capacitor is $U_{in} = \int VdQ$ from the charging curve (the areas of I and II in Figure 31(b)) and the total discharged electric energy to a load is $U_{out} = \int VdQ$ from the discharge curve (the area I). The area II represents the total energy loss due to various processes. Thus, the energy storage efficiency can be expressed as the ratio between area I and the sum of area I and II. Here, the QV curves of Figures 31(c) and (d) are direct conversion of data in Figure 31(a), where $Q = \int Idt$ and I is the current. For an ideal capacitor (with very little loss), the QV curves for the charge/discharge processes should overlap. Figure 31(c) presents the QV curves of the asymmetric cell with different scan rates. Figure 31(d) shows the energy storage efficiency derived from Figure 31(c) which shows a near 90% efficiency at 10 mV s^{-1} scan rate, indicating a near ideal capacitor behavior of the asymmetric supercapacitor. As the scan rate

increases, the loss is also increased, as reflected by the decrease of energy efficiency with scan rate. For the comparison, the coulombic efficiency is also presented in Figure 31(d), which stays nearly a constant in the same scan rate range.

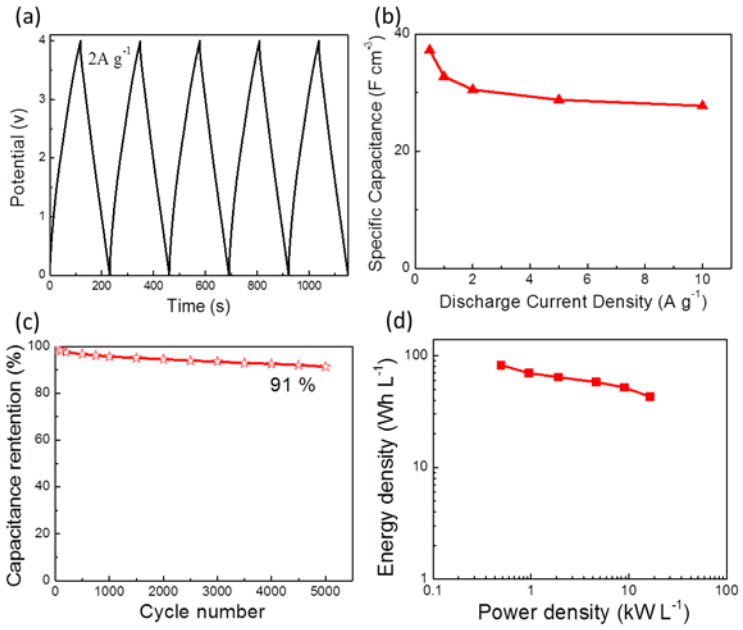

Figure 32 Galvanotatic performance of asymmetric cell. (a) Galvanostatic charge/discharge curves of device at a current density of 2 A g^{-1}. (b) Cell volumetric capacitances of cell at different discharge current densities. (c) Cycle life of the asymmetric supercapacitor under a voltage of 4 V at a current density of 5 A g^{-1} in 2 M $BMIBF_4$/PC electrolyte. (d) Volumetric Ragone plot of asymmetric cell.

To evaluate the capacitive performance of the asymmetric capacitor further, galvanostatic charge/discharge curves at different current densities were also characterized. The galvanostatic cycles at alternate charge/discharge current densities of 2 A g^{-1} and –2 A g^{-1} were presented in Figure 32(a). It should be noted that the current densities are based on the total mass of both electrodes. The symmetric charge/discharge processes indicate the high energy storage efficiency. Figure 32(b) presents the cell volumetric capacitance at different discharge current densities. It should be pointed out that the calculated cell capacitance was based on the total volume of the active materials (including two electrodes and separator) because it is not meaningful to deduce the specific capacitance of a single electrode for the asymmetric supercapacitor. The cell capacitance decreased from 37.2 F cm^{-3} to 27.7 F cm^{-3} as the discharge current density increases from 0.5 A g^{-1} to 10 A g^{-1}, indicating a good capacitance retention. The cycling stability of A-PEODT/CNTs// ultrahigh density A-CNTs asymmetric supercapacitor was investigated by continuously cycling the galvanostatic charge/discharge process between 0 and 4 V at a current density of 5 A g^{-1}. As shown in Figure 32(c), the asymmetric cell shows a 91% capacitance retention after 5000 cycles. The small capacitance loss (~ 9%) is probably caused by the volume change during the charge/discharge process of PEDOT/A-CNTs electrode.

The volumetric energy and maximum power densities are also evaluated for the asymmetric supercapacitors, based on Equation (5) and Equation (4). The asymmetric cells exhibit both high volumetric and gravimetric maximum power density and energy density, which are 130.6 kW L^{-1} (269.4

kW kg^{-1}) and 82.8 Wh L^{-1} (170.7 Wh kg^{-1}), respectively, and are higher compared with symmetric supercapacitors with the ultrahigh density A-CNTs (25 kW L^{-1} / 75 Wh L^{-1}), or CP-ACNTs (35.24 kW L^{-1},11.22 Wh L^{-1}), mainly due to the higher operation voltage in the asymmetric configuration. The volumetric Ragone plots (energy density versus average power density) of asymmetric cell are exhibited in Figure 32(d). It should be mentioned that the average power density in the Ragone plot is different from the maximum power density. The average power density can be obtained by

$$P = E/\Delta t \tag{10}$$

where Δt is discharge time.

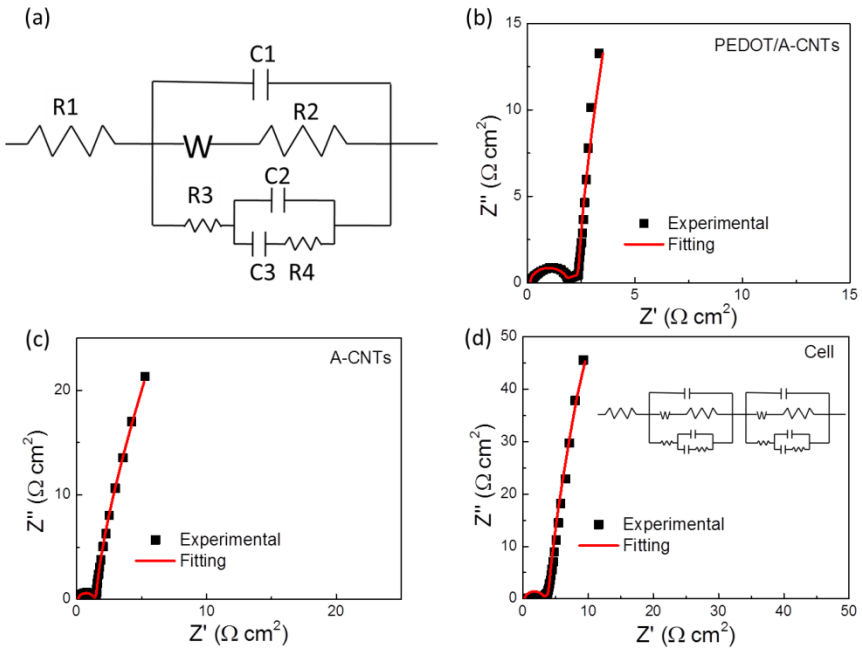

Figure 33. Equivalent circuit fitting for both electrodes and cell. (a) Equivalent impedance circuit of each electrode. Nyquist plot and fitting curve for (b) PEDOT/A-CNTs electrode, (c) ultrahigh density A-CNTs electrode and (d) asymmetric cell.

In order to investigate the influence of PEDOT coating on the A-CNTs and develop understanding of the working mechanisms of pseudocapacitor and EDLC type electrodes, an equivalent circuit model shown in Figure 33(a) is utilized to simulate the electrochemical impedance spectroscopies (EIS) of the two electrodes and the asymmetric cell. In this model, R1 is the internal resistance of electrode related to the conductivity of electrolyte, the Ohmic resistance of the electrode materials, and resistance in the separator, and the contact resistances between active materials and current collector. C1 is the interface contact capacitance between the active material and gold current collector. A_w is the Warburg diffusion element attributed to diffuse ion storage at low frequency in the interface between electrode and electrolyte. The Warburg diffusion impedance can be expressed as $Z_w = A_w/(j\omega)^{0.5}$, where A_w is the Warburg coefficient, ω is the angular frequency. When the applied voltage is small (~k_BT/e), the Warburg coefficient is inversely proportional to the electrode area (see the supporting materials),

$$A_W = \frac{\alpha}{neA\sqrt{D}} \tag{11}$$

where n is the valence of the mobile ions, A is the electrode area, α is a coefficient, and D is the diffusion coefficient. R2 is the interface resistance between electrode and electrolyte. R3 is the charge transfer resistance. C2 represents the double layer capacitance related to the porous electrode. C3 is the pseudocapacitance attributed the conformal coating of PEDOT. The total capacitance of PEDOT/A-CNTs electrode should be expressed as C2+C3. Due to the porous surface of two electrodes, constant phase element (CPE) is used for C2 in the model. The impedance of CPE is defined as $Zcpe = 1/T(jw)^n$, where T is the frequency independent constant with dimensions of $(F\ cm^{-2})^n$ related to the roughness and pseudocapacitive kinetics of electrode, n can be calculated from the slope of log Z vs. log f whose value range from -1 to 1. If n=0, the CPE is a pure resistor, n =1, CPE is a pure capacitor, n=-1, CPE behaves as an inductor. R4 represents the faradaic resistance. Nyquist plots of two electrodes in the frequency range of 100 kHz to 10 mHz at open circuit potential with a 5 mV perturbation signal are shown in Figure 33(b) and 33(c), respectively. Both plots show a sharp increase of the imaginary part in the low frequency region and a semicircle in the high frequency region. The semicircle behavior is attributed to charge transfer resistance of the electrodes, while the sharp increase of the imaginary part is due to the capacitive behavior of the electrode. The fittings to the EIS of both electrodes are also represented in Figure 33(b) and 33(c) as the solid curves, showing that the equivalent circuit of Figure 33(a) can fit the impedance spectroscopy of both electrodes very well. The fitting parameters are listed in Table 3 for comparison.

Electrode	R1 (Ω cm²)	C1 (F cm⁻²)	A_w (Ω s$^{-0.5}$cm²)	R2 (Ω cm²)	R3 (Ω cm²)	C2 (F cm⁻²)	n	C3 (F cm⁻²)	R4 (Ω cm²)
PEDOT/A-CNTs	0.15	0.001	43.33	14.5	1.91	0.19	0.90	0.70	0.74
A-CNTs	0.14	0.001	28.73	6.67	1.39	0.36	0.95	0.11	0.89

Table 3. Fitting parameters for the EISs of two electrodes.

As shown in the Table 3, in the high frequency range, the internal resistances of two electrodes show similar small R1. R1 for the PEDOT/A-CNTs electrode is a little larger because of the higher resistance of PEDOT compared with that of pure ultrahigh density A-CNTs. In the medium frequency region, the larger Warburg coefficient, interface resistance and charge transfer resistance for the PEDOT/A-CNTs electrode compared with those for the A-CNTs electrode indicate the pseudocapacitor redox process. At the low frequency, the double layer capacitance and pseudocapacitance for PEDOT/A-CNTs electrode are 0.19 and 0.70 F cm^{-2}, indicating that the faradaic charge/discharge of PEDOT coating layer plays an important role in contributing to the total capacitance. For the A-CNTs electrode, the double layer capacitance is 0.36 F cm^{-2}. It is noted that the small "psedudocapacitance" of 0.11 F cm^{-2} for the ultrahigh density A-CNTs electrode may come from the slow diffusion process in the small pore size of the electrode. It can be found that the fitting capacitance values are consistent with those calculated from galvanostatic measurements (the values in F/cm^2 can be converted to that in F/cm^3 by dividing them with the electrode thickness of 0.210 mm for PEDOT/A-CNTs electrode and 0.25 mm for ultrahigh density A-CNTs electrode). The large value of n (larger than 0.9) also indicates the porous structure of ultrahigh density A-CNTs and composite electrode. By combining the two sets of fitting parameters (Table 3) for the two individual electrodes

electrically in series, the data for the asymmetric cell can be fitted very well without adjustable parameters, as shown in Figure 33(d) in the whole frequency range, indicating the optimized design of the asymmetric cell.

In summary, an asymmetric supercapacitor with high electrochemical performance has been developed with conformal coating of PEDOT on A-CNTs as the negative and the ultrahigh density A-CNTs as the positive in 2 M $BMIBF_4$/ PC electrolyte. The positive and negative electrodes materials are individually tailored and work synergistically together in the asymmetric cell configuration so that the cell can be operated under the high operation voltage of 4 V to achieve energy and power densities with a long cycle life. Moreover, the EIS of each electrode is modeled by equivalent circuit elements to describe quantitatively the functions of pseudocapacitor and EDLC directly. The EIS of the asymmetric cell is also simulated based on the parameters from two electrodes which demonstrate the optimized asymmetric design.

4. Publications

Yang Liu, Caiyan Lu, Stephen Twigg, Mehdi Ghaffari, Junhong Lin, Nicholas Winograd, Q. M. Zhang. Direct Observations of Space Charge Layers Near Electrodes in Ionic Polymer Actuators Containing Ionic Liquids by ToF-SIMS. *Scientific Reports*, 3, 973 (2013).

Mehdi Ghaffari, Yue Zhou, Haiping Xu, Minren Lin, TaeYoung Kim, Rodney S. Ruoff and Q. M. Zhang. High Volumetric Performance Aligned Nano-Porous Microwave Exfoliated Graphite Oxide (A-aMEGO)-based Electrochemical Capacitors. *Adv. Mater*. 25, 4879 (2013).

N. Lachman, Y. Zhou, M. Ghaffari, D. Bhattacharyya, K. K. Gleason, B. L. Wardle and Q. M. Zhang, "Tailored Aligned-Carbon Nanotube Nanocomposites for Energy Storage", Proc. of the 19th International Conference on Composite Materials (July 28-Aug. 2, Montreal, Canada, 2013).

Yue Zhou, Mehdi Ghaffari, Minren Lin, Ethan M Parsons, Yang Liu, Brian L. Wardle, Q. M. Zhang. High volumetric electrochemical performance of ultra-high density aligned carbon nanotube supercapacitors with controlled nanomorphology. *Electrochimica Acta*, 111, 608 (2013)

Mehdi Ghaffari, Suppanat Kosolwattana,Yue Zhou, Noa Lachman, Minren Lin, Dhiman Bhattacharya, Karen K. Gleason, Brian L. Wardle,and Q. M. Zhang. Highly Efficient Hybrid Supercapacitor Materials from Conformally Coated Aligned Carbon Nanotubes with Poly (3,4-ethylenedioxythiophene). *Electrochimica Acta*, 112, 522 (2013).

Yue Zhou, Noa Lachman, Mehdi Ghaffari, Haiping Xu, Dhiman Bhattacharya, Pouria Fattahi, Mohammad Reza Abidian, Karen K. Gleason, Brian L. Wardle, and Q. M. Zhang. A high performance hybrid asymmetric supercapacitor via nano-scale morphology control of graphene, conducting polymer, and carbon nanotube electrodes. *Journal of Materials Chemistry A*, 2, 9946 (2014).

Minho Kim, Fan Xu, Jin Hong Lee, Cheolsoo Jung, Soon Man Hong, Q. M. Zhang and Chong Min Koo. A fast and efficient pre-doping approach to high energy density lithium-ion hybrid capacitors. *Journal of Materials Chemistry A*, 2, 10029 (2014)

Noa Lachman, Haiping Xu, Yue Zhou, Mehdi Ghaffari, Minren Lin, Dhiman Bhattacharyya, Asli Ugur, Karen K Gleason, Q. M. Zhang, and Brian L Wardle. Tailoring Thickness of Conformal Conducting Polymer Decorated Aligned Carbon Nanotube Electrodes for Energy Storage. *Advanced Materials Interfaces*, DOI: 10.1002/admi.201400076 (2014).

Yue Zhou, Haiping Xu, Noa Lachman, Mehdi Ghaffari, Shan Wu, Yang Liu, Asli Ugur, Dhiman Bhattacharya, Karen K Gleason, Brian L Wardle, and Q. M. Zhang, Advanced Asymmetric Supercapacitor Based on Conducting Polymer and Aligned Carbon Nanotubes with Controlled Nanomorphology. *Nano Energy*, In press (2014)

5. Presentations:

Q. M. Zhang. Electric Double Layer Based Ionic Electroactive Devices. 4th International Conference Smart Materials, Structures, and Systems. Montecatini, Italy (June, 2012) (Invited).

Q. M. Zhang. Understanding ion transport and storage in Ionic Electroactive Polymer Membranes. 63rd Annual Meeting of the International Society of Electrochemistry, Prague (August, 2012) (Invited).

Mehdi Ghaffari, Yue Zhou, Yang Liu, Jiping Cheng, Roberto Guzmán de Villoria, Brian L. Wardle and Q. M. Zhang, Ultra-high Density Aligned Carbon Nanotube with Controlled Nano-morphology for Supercapacitors, America Physical Society, March 2012 Meeting, Boston, MA.

Yue Zhou, Ran Zhao, Yang Liu, Mehdi Ghaffari, Minren Lin, Q. M. Zhang. Equivalent Circuit Modeling of Ionomer and Ionic Polymer Conductive Network Composites. 44th International Union of Pure and Applied Chemistry Polymer Congress. Blacksburg, VA (June, 2012).

Qiming Zhang and Brian L. Wardle, Ultrahigh Volume Content Aligned Carbon-Nanotube Nanocomposite Energy Conversion and Storage Devices, NECST Consortium semi-annual meeting, Nov. 28, 2012, Cambridge, MA.

Yue Zhou, Noa Lachman, Mehdi Ghaffari, Haiping Xu, Brian L. Wardle, and Q. M. Zhang, Nano-scale Morphology Control of Graphene, Conducting Polymer, and Carbon Nanotube Electrodes for High Performance Energy Storage, 224th ECS meeting, October 27- November 1, 2013, San Francisco, CA, USA.

Mehdi Ghaffari, Yue Zhou, Minren Lin, Haiping Xu, TaeYoung Kim, Rodney S. Ruoff, and Q. M. Zhang, High Volumetric Performance Aligned Nano-Porous Graphene-based Electrochemical Capacitors, 224th ECS meeting, October 27- November 1, 2013, San Francisco, CA, USA.

Yue Zhou, Haiping Xu, Noa Lachman, Mehdi Ghaffari, Brian L. Wardle, and Q. M. Zhang, Asymmetric Supercapacitor Based on Conducting Polymer and Aligned Carbon Nanotubes with Controlled Nanomorphology, 15th International Symposium on Electrets (ISE) meeting, August 10-13, 2014, Baltimore, MD, USA.

B. L. Wardle, September 2013, Plenary: “Hierarchical Nanoengineered Structural Advanced Composites – Fundamentals and Applications,” 6th International Conference on Carbon NanoParticle Based Composites – CNPComp2013, Dresden, Germany.

B. L. Wardle, December 2013, Invited Talk: "Transport in Aligned Nanotube Arrays as Model Systems: Phonon, Electron, Ion, Particle, and Polymer Studies," Symposium TT: Transport Properties in Nanocomposites, Fall Annual Meeting of the Materials Research Society (MRS), Boston, MA.